

# Tessellation codes: encoded quantum gates by geometric rotation

Yixu Wang,<sup>1,\*</sup> Yijia Xu (许逸霞),<sup>2,3,†</sup> and Zi-Wen Liu<sup>4,‡</sup>

<sup>1</sup>*Institute for Advanced Study, Tsinghua University, Beijing, 100084, China*

<sup>2</sup>*Joint Center for Quantum Information and Computer Science,  
University of Maryland, College Park, Maryland 20742, USA*

<sup>3</sup>*Institute for Physical Science and Technology, University of Maryland, College Park, Maryland 20742, USA*

<sup>4</sup>*Yau Mathematical Sciences Center, Tsinghua University, Beijing, 100084, China*

(Dated: April 22, 2025)

We utilize the symmetry groups of regular tessellations on two-dimensional surfaces of different constant curvatures, including spheres, Euclidean planes and hyperbolic planes, to encode a qubit or qudit into the physical degrees of freedom on these surfaces, which we call tessellation codes. We show that tessellation codes exhibit decent error correction properties by analysis via geometric considerations and the representation theory of the isometry groups on the corresponding surfaces. Interestingly, we demonstrate how this formalism enables the implementation of certain logical operations through geometric rotations of surfaces in real space, opening a new approach to logical quantum computation. We provide a variety of concrete constructions of such codes associated with different tessellations, which give rise to different logical groups.

## I. INTRODUCTION

In the pursuit of scalable quantum technologies such as quantum computing, quantum error correction is a challenging yet essential task. Besides the robust storage of the encoded quantum information, efficient and robust manipulation of encoded quantum information through logical operations is a crucial but nontrivial problem. Consequently, designing quantum error-correcting codes with desired logical gate sets emerges as a pressing problem that has garnered substantial attention, spanning a variety of important settings, including topological codes [1–7], product codes [8, 9], covariant codes [10–17], bosonic codes [18–25], dynamical codes [26–28], fusion-based quantum computing [29, 30].

In this work, we adopt a geometric perspective and discuss a framework of quantum codes whose code states are extended in real space. Here, symmetries of the space can be utilized as a resource. The Gottesman–Kitaev–Preskill (GKP) code [18] utilizes the translation symmetry on flat space. We explore the rotational symmetries of two-dimensional surfaces with different curvatures and demonstrate how they enable implementations of logical quantum gates by geometric rotations which are expected to be fault-tolerant and experimentally feasible. While codes that allow gate implementation via rotations on spheres have been explored [31–34], we approach the code construction from the new perspective of regular triangle tessellations and propose a more general geometric formalism for constructing quantum codes, termed *tessellation codes*, that encompasses surfaces with different curvatures, including spheres, Euclidean planes and hyperbolic planes. Leveraging the connections between the group structures of the logical gate sets and the triangle groups of the tessellations, our tessellation codes can support representations of logical gate sets realizable by geometric rotations (see also Refs. [32, 33, 35–39] for different perspectives of such “covariant encodings”

that have been under intensive study recently). Relatedly, recent work has explored extending transversal gates through qubit lattice rotations within the framework of fold-transversal logical gates in a discrete-variable setting [40].

On the other hand, our formalism utilizes lattices defined by tessellation. In this regard, our constructions also generalize the GKP codes [41, 42] based on lattices on curved spaces. We note that some specific kinds of surface tessellation were used to construct microscopic models of holography [43–45] and quantum codes [46] in different setups in previous studies.

Specifically, in our tessellation codes, the codewords are superpositions obeying patterns of surface tessellation and the logical gates correspond to rotational symmetries acting on the tessellation. By choosing different tessellations, we obtain quantum codes with different logical gate sets and error correction properties. To supplement the general theory, we shall provide several examples built from our formalism to illustrate the interplay among lattice symmetries, logical gate sets, and error correction.

Of particular interest are hyperbolic planes, whose exotic features may induce striking implications for coding theory and physics. This has been seen in classical codes [47], the hyperbolic surface codes that overcome the Bravyi–Poulin–Terhal (BPT) bound [48–50], band theory for non-abelian lattices [51–54], and exotic phases of matter [55–59]. The present work provides the first examples of continuous-variable (CV) codes on hyperbolic planes. Especially, the rich (infinite) types of regular tessellations on hyperbolic planes enable us to realize a variety of logical gate sets, including the qudit Pauli group, the single-qubit Clifford group, the binary icosahedral group and even the universal single-qubit gate set. Moreover, hyperbolic plane can be viewed as the parameter space of squeezed states. The rotation and hyperbolic translations can be realized by Gaussian operations such as phase gates and two-mode squeezing operations. We anticipate that our formalism can shed new light on code construction in bosonic systems.

The paper is organized as follows. We first overview the group structure of Pauli and Clifford groups. We present their underlying connection to the triangle groups in Sec. II.

\* wanyixu@mail.tsinghua.edu.cn

† yijia@umd.edu

‡ zwliu0@tsinghua.edu.cn

In Sec. III, we set up the framework of our code construction, including the encoding map III A, the error model and its correction strategy III B. In Sec. IV, we provide several examples built from our formalism in different surfaces and tessellations, including examples on the sphere (Example 1), Euclidean plane (Examples 2, 3), and hyperbolic space (Examples 4, 5, 6). These examples exhibit the interplay among lattice symmetries, logical gate sets, and error correction. In Sec. V, we discuss the potential of our framework to realize universal logical gates.

## II. GROUP STRUCTURE

In this work, we use group presentation  $G = \langle A|R \rangle$  [60] which comprises two parts—generators  $A$  and the relation of generators  $R$ —to describe a group  $G$ . For example, the qubit Pauli group has presentation

$$\mathcal{P}_{\text{qubit}} = \langle X, Z | X^2 = Z^2 = (XZ)^4 = \mathbb{1} \rangle. \quad (1)$$

For a qudit of general dimension  $d \geq 3$ , its Pauli group is generated by  $X = \sum_{j=0}^{d-1} |j+1\rangle\langle j|$  and  $Z = \sum_{j=0}^{d-1} \omega^j |j\rangle\langle j|$ , where  $\omega = e^{i\frac{2\pi}{d}}$ . The group presentation of qudit Pauli group is

$$\mathcal{P}_{\text{qudit}} = \langle X, Z | X^d = Z^d = \Omega X \Omega^{-1} X^{-1} = \Omega Z \Omega^{-1} Z^{-1} = \mathbb{1} \rangle. \quad (2)$$

Here  $\Omega \equiv XZ X^{-1} Z^{-1}$  is the group commutator of  $X$  and  $Z$ . The last two relations mean that  $\Omega$  is a central element. One can derive  $\Omega^d = \mathbb{1}$  with these relations. Therefore,  $\Omega$  is identified as  $e^{i\frac{2\pi}{d}} \mathbb{1}$  in a unitary representation of the qudit Pauli group. One can also derive  $(XZ)^d = \mathbb{1}$  for odd integer  $d$  and  $(XZ)^{2d} = \mathbb{1}$  for even integer  $d$  from Eq. (2).

There are various realizations of the single-qubit Clifford group that are equivalent up to global phases. An example presented in Ref. [36] is generated by

$$S = \begin{pmatrix} e^{i\frac{\pi}{4}} & 0 \\ 0 & e^{-i\frac{\pi}{4}} \end{pmatrix}, U = \frac{1}{\sqrt{2}} \begin{pmatrix} e^{i\frac{\pi}{4}} & e^{i\frac{\pi}{4}} \\ -e^{-i\frac{\pi}{4}} & e^{-i\frac{\pi}{4}} \end{pmatrix}. \quad (3)$$

We have  $S^4 = U^3 = (US)^2 = -\mathbb{1}$ . This choice of the single-qubit Clifford group has 48 elements. Its presentation is

$$\mathcal{C} = \langle S, U | S^8 = U^6 = (US)^4 = S^4 U^3 = S^4 (US)^2 = \mathbb{1} \rangle. \quad (4)$$

Regular triangle tessellations of two-dimensional surfaces are characterized by three positive integers  $\{p, q, r\}$ , which represent three internal angles  $\{\frac{2\pi}{p}, \frac{2\pi}{q}, \frac{2\pi}{r}\}$  of the unit triangle. These three integers also determine the symmetry group of the tessellation, known as the triangle group. A triangle group [61] has three generators which are reflections along each edge of a triangle, labeled by their corresponding edges as  $f_a, f_b, f_c$ . We denote the triangle group of the tessellation  $\{p, q, r\}$  as  $\Delta(p, q, r)$ . Its presentation is

$$\langle f_a, f_b, f_c | f_a^2 = f_b^2 = f_c^2 = (f_b f_c)^p = (f_c f_a)^q = (f_a f_b)^r = \mathbb{1} \rangle. \quad (5)$$

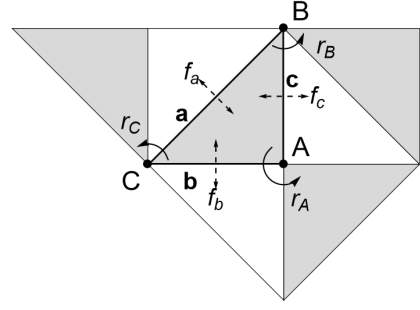


FIG. 1. The  $\{2, 4, 4\}$  tessellation on the plane is used to illustrate the action of the generators of the triangle and proper triangle groups. Generators of other  $\{p, q, r\}$  groups act similarly geometrically. The dashed double-arrow lines represent reflections along the edges it crosses, and the solid single-arrow lines represent rotations.

An index-2 subgroup is called the proper triangle group, denoted as  $\bar{\Delta}(p, q, r)$ . Its elements are products of even numbers of reflection generators. By redefining  $r_A \equiv f_b f_c$ ,  $r_B \equiv f_c f_a$ ,  $r_C \equiv f_a f_b = (r_A r_B)^{-1}$ , the presentation of the proper triangle group can be written as

$$\bar{\Delta}(p, q, r) = \langle r_A, r_B | r_A^p = r_B^q = (r_A r_B)^r = \mathbb{1} \rangle. \quad (6)$$

Here  $r_A = f_b f_c$  is the rotation around the angle  $A$  defined by sides  $b$  and  $c$  in the direction from  $c$  to  $b$  by  $\frac{2\pi}{p}$ .  $r_B$  and  $r_C$  have similar geometric meanings, as depicted in Figure. 1.

The integers label the types of the tessellations. Their reciprocal sum is related to the curvature of the surfaces,

$$\frac{1}{p} + \frac{1}{q} + \frac{1}{r} \begin{cases} > 1 & \Rightarrow \text{sphere,} \\ = 1 & \Rightarrow \text{Euclidean plane,} \\ < 1 & \Rightarrow \text{hyperbolic plane.} \end{cases} \quad (7)$$

We observe that single-qudit Pauli, Clifford, and proper triangle groups are all generated by two generators and specific relations that certain products of generators equal to the identity element. The structural similarities between the presentation of proper triangle groups (6) and the Pauli group (2) or the single-qubit Clifford group (4) motivate us to realize logical qubit gates via geometric manipulations.

The presentations of the Pauli or Clifford groups have extra relations compared to their proper triangle group counterparts. From an algebraic perspective, imposing extra relations  $R$  is described as the quotient of the triangle group by the normal subgroup called the normal closure of  $R$ . The normal closure is generated by the generators of the form  $R^\Delta = \{g^{-1} r g, g \in \bar{\Delta}, r \in R\}$ . Geometrically, these extra relations set identification relations to the lattice points of the tessellation, thus specifying unit cells of the lattice. The normal closure is the translation group in lattice theory and is often denoted as  $\Gamma$ . In the context of quantum error correction theory, it plays a similar role to the stabilizer group in the non-commuting case, so we call  $\Gamma$  the generalized stabilizer group. The relation between the logical group  $G$ , the proper triangle group  $\bar{\Delta}$ , and the generalized stabilizer group  $\Gamma$  is

$$G = \bar{\Delta} / \Gamma. \quad (8)$$

### III. GENERAL FORMALISM

#### A. Encoding strategy

We now explain the general framework for constructing tessellation codes that enable geometric realizations of logical gates. The physical degree of freedom is a free massless two-dimensional boson on the corresponding surfaces. The physical Hilbert space  $\mathcal{H}_P$  corresponds to the space of wavefunctions defined on these surfaces. The logical degree of freedom is a qubit or a qudit, which can be understood as a virtual system that hosts the logical group actions as we shall discuss. The corresponding logical space  $\mathcal{H}_L$  is the  $d$ -dimensional vector space for qudits. Our goal is to construct a covariant encoding for group  $G$ , where a  $d$ -dimensional unitary representation  $\rho_L(g)$  acting on the logical space  $\mathcal{H}_L$  is implemented by a geometric rotation  $\rho(g)$  acting on the physical space  $\mathcal{H}_P$  for  $\forall g \in G$ . For the Euclidean and hyperbolic cases, each logical  $g$  can be written as  $\rho(g) = \Gamma g_0 = \sum_{\gamma \in \Gamma} \gamma g_0$ , for an arbitrary coset representative  $g_0$  under the quotient of Eq. (8).

We now construct the positional configurations of the codewords. As the encoding map is covariant for  $G$ , it should involve the structure of a linear map intertwining between representations  $V = \sum_{g \in G} \rho_L(g)^{-1} \otimes \rho(g)$ . The general encoding map  $\mathcal{E}$  takes the form in Ref. [36]. The codeword  $|\bar{k}\rangle \in \mathcal{H}_P$ , which represents the logical state  $|k\rangle \in \mathcal{H}_L$  to be encoded, can be written as

$$|\bar{k}\rangle \equiv \mathcal{E}(|k\rangle) \propto \sum_{g \in G} \langle \Sigma | \rho_L(g)^\dagger | k \rangle \rho(g) | \text{init} \rangle. \quad (9)$$

Here the states  $|\Sigma\rangle \in \mathcal{H}_L$  and  $|\text{init}\rangle \in \mathcal{H}_P$  are chosen such that  $\langle \Sigma | V | \text{init} \rangle \neq 0$ . In most cases, we choose  $|\Sigma\rangle = |0\rangle \in \mathcal{H}_L$ . For simplicity, we take the initial state  $|\text{init}\rangle$  as a delta function state localized at a given point  $p_i$  on the two-dimensional surface. We write  $|\text{init}\rangle = |p_i\rangle$  hereafter, which will be parameterized in spherical, Cartesian, and hyperbolic polar coordinates for sphere, Euclidean, and hyperbolic planes respectively. The collection of delta functions for a given codeword is called its configuration.  $|p_i\rangle$  can be chosen arbitrarily inside or on the edges of a unit triangle (see Fig. 1) for code construction, except for the vertices. The collection of delta functions for a given codeword is called its configuration. Different choices of  $|p_i\rangle$  induce different code constructions. Whether  $|p_i\rangle$  can be put on vertices of the triangle and how choices of  $|p_i\rangle$  affect the code performance are discussed in detail in Appendix. A.

#### B. Error model and correction

We discuss error models on each type of surface and introduce parameters to characterize the code performance. The position error is modelled by an orientation-preserving isometric transformation of the plane and reflects the imprecision of logical operation implementations or unexpected vibration of the system. We define the robustness against position error by resolution  $d_x$ , which is half of the minimum distance

between two points in the code configurations. The momentum errors are modelled by the eigenfunctions of the Laplacian operators on each surface type, which are labelled by two indices for two-dimensional surfaces and form bases of the irreducible representations of the isometry group. Physically, the eigenvalues are the kinetic energies of the modes. Momentum errors model the unexpected energy excitations of the physical system. Mathematically, they are bases of irreducible representations of the isometry group. In Table I, we list different types of position and momentum errors on corresponding surfaces. We denote an error operator as  $\hat{E}_{r,n}$ , in which  $r$  labels the representation and  $n$  labels the  $n$ -th basis of the vector space carrying the representation. The error correction properties of codes from our framework can be analyzed based on these interpretations. In the main text, we highlight the logical operation aspects, while a more detailed discussion on error correction is provided Appendix. A and B

The code's performance against position errors can be naturally characterized by geometric parameters. One such parameter is one-half of the minimal distance among pairs of adjacent points, which we call the resolution  $d_x$ . For an isometry  $g$  which transforms a point up to a finite distance,  $\|p_i - gp_i\| \leq d_g < \infty$ , if  $d_g < d_x$ , then the error  $g$  is correctable. The resolution  $d_x$  indeed depends on codeword configurations, through the choice of  $|p_i\rangle$  in Eq. (9). In Appendix. A, we show how to determine the  $|p_i\rangle$  that gives the optimal resolution configuration of a given tessellation.

Correcting position error is determining an unknown isometry. In principle, there are at most two fixed points for isometries on a sphere and at most one for isometries on an Euclidean plane or a hyperbolic plane (excluding points at infinity). Therefore, we can measure two points (or three points on a sphere if the first two measurement results are antipodal) and compare their positions before and after the isometry. The unknown isometry should be solved up to an element of the generalized stabilizer group. We can then apply the inverse isometry to correct the error. Every measurement gives one position and we need to at least measure twice.

The configurations of noiseless codewords are known and denoted as set  $L$ . The syndrome measurement gives the positions of two points  $p_1^{(m)}, p_2^{(m)}$  of the noisy state. The error correction amounts to determining their original positions and the error  $g_e$ . We examine different ansatz of isometries that take the two positions back to one pair of points in the original configuration  $L$ . We denote all such isometries as the set  $Q = \{g | gp_1^{(m)}, gp_2^{(m)} \in L\}$ . If a probability distribution  $\mu$  of the noise group elements is given, we may use the maximal probability decoder to find the most probable error  $g_e$ :

$$g_e = \operatorname{argmax}_{g: g \in Q} \mu(g). \quad (10)$$

The momentum errors are basis of irreducible representations of the isometry group. We denote momentum error operator as  $\hat{E}_{r,n}$ , in which  $r$  labels the representation and  $n$  labels the  $n$ -th basis of the vector space carrying the representation. In correspondence with Table. I,  $r \rightarrow \ell$  and  $n \rightarrow m$  for the spherical errors,  $r \rightarrow (k_x, k_y)$  for the Euclidean errors,

and  $r \rightarrow r$ ,  $n \rightarrow n$  for the hyperbolic errors. The analysis of the Knill–Laflamme error correction conditions [62] of momentum errors can be unified with the help of the representation theory of the isometry groups. Consider the pairs of errors  $\hat{E}_{r_1, n_1}$ ,  $\hat{E}_{r_2, n_2}$ , if  $(r_1, n_1) = (r_2, n_2)$ , the error correction condition is always satisfied. For the cases where  $(r_1, n_1) \neq (r_2, n_2)$ , most of them also satisfy the error correction condition, exactly due to the consequence of the representation theory of the generalized stabilizer group by Schur’s lemma. It is straightforward to calculate the violating pairs for the codes on the sphere and Euclidean plane but harder for those on the hyperbolic plane. We conjecture that the error correction performance against momentum error can be characterized by the first non-trivial eigenvalue of the Laplacian of the compact manifold after the quotient of the generalized stabilizer group. We collect the representation-theoretic analysis of error correction conditions of momentum errors in Appendix B.

#### IV. CASE STUDIES

In the following, we introduce some representative examples of codes associated with spherical, planar, and hyperbolic tessellations derived from the above general framework, with certain groups of logical operations realized by geometric rotations. There are infinitely many different regular tessellations on the hyperbolic plane enabling us to realize a wide range of logical gate sets. We only present three examples as proof of principle. We describe each code by the type of tessellation, the generalized stabilizers, the logical operator generators, and the code performance against position and momentum errors. To lighten the notation, we take the curvature radius of both sphere and hyperbolic plane to be 1. For the Euclidean plane, the side length of the isosceles right triangle is 1. So is the side length of the equilateral triangle. We summarize the parameters and key information of all codes in Table II. In the main text, we present the codewords configurations of the examples with a particular choice of  $|p_i\rangle$ . The general codewords and their relations to other codes are given in Appendix C.

	Sphere	Euclidean plane	Hyperbolic plane
Isometry group	SO(3)	E(2)	PSL(2, $\mathbb{R}$ )
Position errors	Rotation along any axis	Translations, rotations	Hyperbolic translations, rotations
Momentum errors	$Y_\ell^m(\hat{\theta}, \hat{\phi}) = P_\ell^m(\cos \hat{\theta})e^{im\hat{\phi}}$	$\exp(i(k_x \hat{x} + k_y \hat{y}))$	$P_{-\frac{1}{2} + is}^n(\cosh \hat{\rho})e^{in\hat{\phi}}$

TABLE I. Different types of position and momentum errors in the table. Position errors are elements of orientation-preserving isometry groups. Momentum errors are the eigenfunctions of the Laplacians of the corresponding surfaces. They are also basis of unitary representations of the isometry group.

	Example 1	Example 2	Example 3	Example 4	Example 5	Example 6
Designated logical group	Qubit Pauli	Qubit Pauli	Qutrit Pauli	$\mathbb{Z}_5$ qudit Pauli	Qubit Clifford	Binary icosahedral
Surface type	Sphere	Euclidean plane	Euclidean plane	Hyperbolic plane	Hyperbolic plane	Hyperbolic plane
Triangle tessellation	$\{2, 2, 4\}$	$\{2, 4, 4\}$	$\{3, 3, 3\}$	$\{5, 5, 5\}$	$\{6, 4, 8\}$	$\{4, 3, 5\}$
Generator identifications	$r_A \rightarrow Z$ $r_B \rightarrow X$ $r_C \rightarrow XZ$	$r_A \rightarrow X$ $r_B \rightarrow Z$ $r_C \rightarrow (XZ)^{-1}$	$r_A \rightarrow Z$ $r_B \rightarrow X$ $r_C \rightarrow (ZX)^{-1}$	$r_A \rightarrow Z$ $r_B \rightarrow X$ $r_C \rightarrow (ZX)^{-1}$	$r_A \rightarrow U$ $r_B \rightarrow (US)^{-1}$ $r_C \rightarrow S$	$r_A \rightarrow \Phi F^{-1}$ $r_B \rightarrow -F$ $r_C \rightarrow -\Phi^{-1}$
Extra relations	—	$r_B^2$	$\Omega r_A \Omega^{-1} r_A^{-1},$ $\Omega r_B \Omega^{-1} r_B^{-1}$	$\Omega r_A \Omega^{-1} r_A^{-1},$ $\Omega r_B \Omega^{-1} r_B^{-1}$	$r_B^2 r_A^3, r_B^2 r_C^4$	$r_B^2 r_A r_B^2 r_A^{-1}$
State configuration	Figure 2	Figure 3	Figure 4	Figure 6	Figure 7	Figure 8
Resolution $d_x$	$\frac{1}{2} \arccos \frac{1}{3}$	$\frac{1}{2}$	$\frac{\sqrt{3}}{2}$	1.6169	0.6605	0.5011

TABLE II. Different properties of the codes constructed in this work. We denote  $\Omega \equiv r_B r_A r_C$ , which is identified as  $XZ X^{-1} Z^{-1}$ , the commutator of the Pauli  $X$  and  $Z$  operator.

**Example 1.** First, we utilize the sphere’s  $\{2, 2, 4\}$  tessellation to realize a qubit code with logical Pauli operations realized by rotations. The  $\hat{\Delta}(2, 2, 4)$  is isomorphic to the qubit Pauli group (1). The most general form of the codewords is presented in Eq. (C1). In Figure 2, the configuration corre-

sponds to the specific choice  $\theta_0 = \arccos \frac{1}{\sqrt{3}}$ ,  $\phi_0 = \frac{\pi}{4}$ . They are on the vertices of a cube. The logical operations are implemented as rotations along different axes. The logical  $Z$  is rotating around the  $x$  axis by  $\pi$ . The logical  $X$  is rotating around the diagonal of the  $x, y$  axis by  $\pi$ . The logical  $XZ$  is



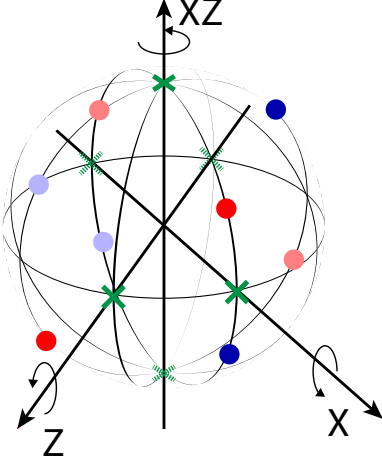


FIG. 2. The constellation of the spherical code in Example 1. The logical 0 state is superposed by the states localized at red and pink points, while logical 1 is by blue and light blue ones. The red and blue points have a coefficient of 1 while the pink and light blue ones have a coefficient of  $-1$ .

to rotate around the  $z$  axis counterclockwise by  $\frac{\pi}{2}$ .

The position error on the sphere is a rotation  $R(\theta, \phi, \alpha)$  around the axis through the point  $(\theta, \phi)$  by an angle  $\alpha$ . Therefore, for any two rotations  $R_1(\theta_1, \phi_1, \alpha_1)$  and  $R_2(\theta_2, \phi_2, \alpha_2)$  with  $\alpha_1, \alpha_2 < \frac{1}{2} \arccos \frac{1}{3}$ , the off-diagonal KL condition  $\langle \bar{0} | R_2^\dagger R_1 | \bar{1} \rangle = \langle \bar{1} | R_2^\dagger R_1 | \bar{0} \rangle = 0$  is always satisfied. For the diagonal condition  $\langle \bar{0} | R_2^\dagger R_1 | \bar{0} \rangle$ ,  $\langle \bar{1} | R_2^\dagger R_1 | \bar{1} \rangle$ , they are also 0, unless the cases in which the axis of the composite rotation  $R_2^\dagger R_1$  exactly passes through one of the configuration point in codeword  $|\bar{0}\rangle$  or  $|\bar{1}\rangle$ . However, in these special cases, because the antipodal points on the rotational axis belong to  $|\bar{0}\rangle$  and  $|\bar{1}\rangle$  respectively for the configuration in Figure 2, the diagonal error correction is still satisfied. Therefore, this code can correct the set of rotations  $R(\theta, \phi, \alpha)$  with arbitrary  $(\theta, \phi)$  and  $\alpha < \frac{1}{2} \arccos \frac{1}{3}$ .

The momentum errors are the spherical harmonics  $Y_\ell^m := Y_\ell^m(\hat{\theta}, \hat{\phi}) = P_\ell^m(\cos \hat{\theta}) e^{im\hat{\phi}}$ . Because the logical  $|\bar{0}\rangle$  and  $|\bar{1}\rangle$  have no spatial overlap, the off-diagonal error correction conditions are always satisfied. For the diagonal part, we evaluate  $\langle \bar{0} | Y_{\ell_1}^{m_1 \dagger} Y_{\ell_2}^{m_2} | \bar{0} \rangle$ ,  $\langle \bar{1} | Y_{\ell_1}^{m_1 \dagger} Y_{\ell_2}^{m_2} | \bar{1} \rangle$  in Appendix B 1. The KL condition is only violated when  $\ell_1 + \ell_2$  is odd and  $(m_1 + m_2) \bmod 4 = 2$ . The lowest uncorrectable pair of the errors is  $Y_1^{0\dagger} Y_2^{\pm 2}$ . Therefore, this code can correct all the momentum errors  $Y_\ell^m$  with  $\ell \leq 1$ .

**Example 2.** The next example is the  $\{2, 4, 4\}$  tessellation on the Euclidean plane. Although the symmetry  $\bar{\Delta}(2, 4, 4)$  is different from the qubit Pauli group, we impose the extra relation  $r_B^2 = \mathbb{I}$ . We obtain a two-dimensional CV code encoding a logical qubit. The logical  $X$  operation is the rotation around the marked vertex along the axis perpendicular to the surface by  $\pi$ . The logical  $Z$  and  $(XZ)^{-1}$  are rotations around their corresponding vertices counterclockwise by  $\frac{\pi}{2}$  respectively. In Figure 3, we illustrate a specific case  $(x_0, y_0) = (\frac{1}{2}, \frac{1}{2})$ . Here

we take the vertex for the rotation  $(XZ)^{-1}$  as the origin, horizontal direction as  $x$  and vertical direction as  $y$ . This code can be viewed as a two-mode GKP code encodes one logical qubit. Each direction is a single-mode GKP code encoding a qubit, while the full code on the plane is a 2-to-1 concatenated qubit code using the two GKP qubits. In appendix C 2 we describe in detail the stabilizers and logical operators from this point of view.

The error correction properties of this code are analogous to those of the GKP codes. For position errors of the translation type, this code can correct any translation of distance less than the resolution  $d_x = \frac{1}{2}$ . The momentum errors are the plane waves. We abbreviate the momentum errors, which are plane waves, as  $\hat{V}_{\vec{k}} \equiv e^{ik_x \hat{x}} e^{ik_y \hat{y}}$ . For a pair of errors  $\hat{V}_{\vec{k}_1}^\dagger \hat{V}_{\vec{k}_2}$ , write  $\Delta k_x \equiv k_{x1} - k_{x2}$  and  $\Delta k_y \equiv k_{y1} - k_{y2}$ . The error correction condition is violated only when both  $\Delta k_x, \Delta k_y$  are odd multiplicities of  $\frac{\pi}{2}$ . Therefore the code can correct any error with  $|\vec{k}| < \frac{\sqrt{2}\pi}{4}$ . The calculation for the momentum error is in Appendix B 2.

**Example 3.** The  $\{3, 3, 3\}$  tessellation can encode a logical qutrit in the plane. As shown in Table II, the qutrit Pauli group is obtained from the  $\bar{\Delta}(3, 3, 3)$  group by adding an extra condition indicating  $\Omega = XZX^{-1}Z^{-1}$  is a central element. The logical gate  $X, Z$  and  $(ZX)^{-1}$  are implemented by rotations around the corresponding vertices by  $\frac{2\pi}{3}$ . Figure 4 shows one unit cell of the codewords with the choice  $|p_i\rangle = |(1, 0)\rangle$ . The explicit code word is shown in Eq. (C6). As described in Appendix C 3, this code has GKP-like stabilizer operators, see Eq. (C7). The GKP-like logical  $Z$  operator can also be obtained. However, the logical  $X$  operator cannot be realized by real space displacement.

For the position error of the translation type, this code corrects translation of distance less than  $d_x = \frac{\sqrt{3}}{2}$ . For the momentum error, the error correction condition is only violated when both  $3\Delta k_x$  and  $\sqrt{3}\Delta k_y$  are multiplicities of  $\frac{2\pi}{3}$  but not multiplicities of  $2\pi$ . It turns out this code can correct mo-

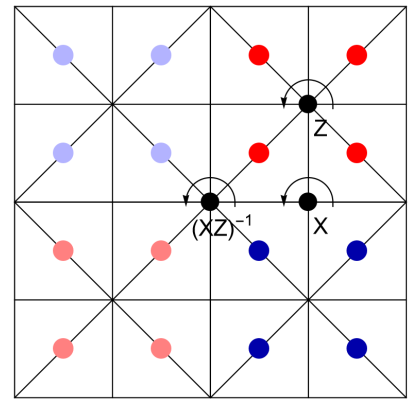


FIG. 3. The unit cell of the constellation of the Euclidean plane code. The colours represent the same as those in Figure 2. The logical operations are implemented by rotation around the corresponding vertices.

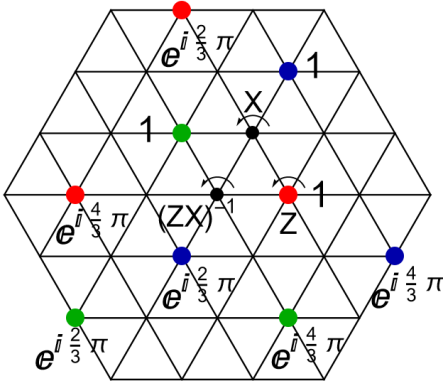


FIG. 4. The unit cell of the constellation of the qutrit code in Example 3. The red, blue and green points consist of the logical  $|0\rangle$ ,  $|1\rangle$ ,  $|2\rangle$  states respectively. The coefficients in the superposition are labelled next to the points. The logical operations are implemented by rotation around the corresponding vertices counterclockwise by  $\frac{2\pi}{3}$ .

momentum errors in any direction with  $|\vec{k}| < \frac{2\pi}{9}$ . The detailed calculation is in Appendix B 3.

**Example 4.** The  $\mathbb{Z}_5$  qudit Pauli group has presentation as in Eq. (2) with  $d = 5$ . It is natural to realize it on a  $\{5, 5, 5\}$  lattice with extra relations, as presented in Table II. The logical gates  $X$ ,  $Z$  and  $(ZX)^{-1}$  are implemented by rotations around the corresponding vertices by  $\frac{2\pi}{5}$ . Figure 6 highlights one unit cell of the codewords if we choose  $|p_i\rangle = |(b, 0)\rangle$ , where  $b = \text{arccosh} \frac{\cos \frac{\pi}{5} + \cos^2 \frac{\pi}{5}}{\sin^2 \frac{\pi}{5}}$  is the distance between the vertices of  $(ZX)^{-1}$  and  $Z$ . For the position error of the translation type, this code corrects translation of distance less than  $d_x = \frac{1}{2} \text{arccosh} ((1 - \cos \frac{2\pi}{5}) \cosh^2 b + \cos \frac{2\pi}{5}) \approx 1.6169$ . Because of the 5-fold rotation symmetry of the hyperbolic lattice, this code can correct any momentum error  $P_{-\frac{1}{2}+ir}^n (\cosh \hat{\rho}) e^{in\hat{\phi}}$  with  $n < 5$ .

Regarding the momentum error's  $r$  index in hyperbolic plane, we note that the surface from the quotient  $\mathbb{H}^2/\Gamma$  is a compact surface, with genus 26 in this example. The Laplacian on this surface has a discrete spectrum, and its first excited eigenvalue  $\lambda_1$  defines the energy gap. We anticipate that any error with eigenvalue less than  $\lambda_1$  should satisfy the error correction condition and be correctable. However, given the generalized stabilizer data, although there is an estimate of the upper bound [63], the exact value of the first positive eigenvalue has no analytic expression and it is highly non-trivial to calculate it numerically for high-genus surfaces. Nevertheless, the energy gap  $\lambda_1$  provides a non-zero notion of “distance of momentum error”. This argument applies to codes on hyperbolic planes, including Examples 4, 5 and 6.

**Example 5.** The group presentation of the Clifford group in Eq. (4) is analogous to the proper triangle group  $\tilde{\Delta}\{6, 4, 8\}$ . We can use this tessellation to construct codes with geometric logical Clifford operations. In Figure 7 we show the codeword configurations of the logical  $|0\rangle$  and  $|\bar{1}\rangle$ . Here we

choose  $|p_i\rangle = |(b, 0)\rangle$ , where  $b = \text{arccosh} \frac{\cos \frac{\pi}{4} + \cos \frac{\pi}{8} \cos \frac{\pi}{6}}{\sin \frac{\pi}{8} \sin \frac{\pi}{6}}$  is the distance between the vertices of  $S$  and  $U$ . The logical  $S$  gate is realized by rotation around the corresponding vertex by  $\frac{\pi}{4}$ , while the logical  $U$  gate is realized by rotation around the corresponding vertex by  $\frac{\pi}{3}$ . These gates are defined in Eq. (3). Interestingly, two codewords have positional overlap, but the relative phases guarantee that they have a zero inner product. This is analogous to the logical  $|\pm\rangle$  states of GKP code. For the position error of the translation type, this code corrects translation of distance less than  $d_x = \frac{1}{2} \text{arccosh} ((1 - \cos \frac{\pi}{4}) \cosh^2 \frac{b}{2} + \cos \frac{\pi}{4}) \approx 0.6605$ .

**Example 6.** We can construct a code with the logical binary icosahedral group [37, 64] on the tessellation  $\{4, 3, 5\}$ . This group has 120 elements and contains non-Clifford gates. It can be generated by

$$F = \frac{e^{-i\frac{\pi}{4}}}{\sqrt{2}} \begin{pmatrix} 1 & -i \\ 1 & i \end{pmatrix}, \quad \Phi = \frac{1}{2} \begin{pmatrix} \phi_G + i\phi_G^{-1} & 1 \\ -1 & \phi_G - i\phi_G^{-1} \end{pmatrix}. \quad (11)$$

Here  $\phi_G = \frac{\sqrt{5}+1}{2}$  is the golden ratio. The generators have the relations  $F^3 = \Phi^5 = (\Phi F^{-1})^2 = -1$ . In Figure 7 we show the codeword configurations of the logical  $|0\rangle$  and  $|\bar{1}\rangle$ . Here we choose  $|p_i\rangle = |(b, 0)\rangle$ , where  $b = \text{arccosh} \frac{\cos \frac{\pi}{3} + \cos \frac{\pi}{4} \cos \frac{\pi}{5}}{\sin \frac{\pi}{4} \sin \frac{\pi}{5}}$  is the distance between the vertices of  $-F$  and  $-\Phi^{-1}$ . The logical  $-F$  gate is realized by rotation around the corresponding vertex by  $\frac{2\pi}{3}$ , while the logical  $-\Phi^{-1}$  gate is realized by rotation around the corresponding vertex by  $\frac{2\pi}{5}$ . These gates are defined in Eq. (3). For the position error of the translation type, this code corrects translation of distance less than  $d_x = \frac{1}{2} \text{arccosh} ((1 - \cos \frac{2\pi}{5}) \cosh^2 \frac{b}{2} + \cos \frac{2\pi}{5}) \approx 0.5011$ .

## V. UNIVERSAL GATE SET ON HYPERBOLIC SURFACES

Although the code constructions discussed above mostly focus on finite logical groups, we note that it is possible to realize the universal single-qubit logical gate set within our formalism. Hyperbolic planes admit a special family of tessellations, one or two of the labeling integers  $\{p, q, r\}$  could be  $\infty$ . For example, the  $\{\infty, 2, 8\}$  tessellation has presentation  $r_B^2 = r_C^8 = 1$ . It is natural to identify  $r_B$  with the Hadamard gate  $H$  and  $r_C$  with the  $T$  gate. By imposing the extra relation  $(r_B r_C^2)^3$  commutes with every generator and  $(r_B r_C^2)^{24} = 1$ , the resulting quotient of the proper triangle group is isomorphic to the universal gate set. This indicates the feasibility of using Eq. (9) to construct a code whose entire logical gate set is implemented by geometric rotations. Our construction utilizes infinite-dimensional physical Hilbert spaces to circumvent the limitations on logical gates in finite dimensions. It is compatible with the analysis of codes covariant for continuous groups in Ref. [65].

## VI. DISCUSSION

In this work, we introduced a versatile geometric formalism for constructing continuous variable quantum error-correcting codes whose designated logical gate sets can be realized by spatial rotations, providing new perspectives for designing codes and logical gates. The symmetries of the tessellation lattice and the underlying surfaces play a crucial role in code construction and error correction.

Numerous directions are worth further exploring. First, the error correction protocol warrants a more comprehensive study. Specifically, we discussed the correction for position errors, but the case of momentum errors has not been fully understood and should be further investigated. Second, we would like to further understand the geometric analogues of the Eastin–Knill theorem and its extensions [10–14, 17, 66] that characterize the general interplay between versatility of logical operations for a quantum code and its error correction performance. Third, we expect further studies of the geometric interpretation and physical relevance of magic in similar settings [67–69] to be fruitful. Fourth, the code state written formally in Eq. (9) is unnormalizable for the codes on the Euclidean or hyperbolic planes. It is interesting to study the regularized version of the code and how exact logical gates become approximate under the regularization. Fifth, generalizing our formalism to logical gates among several encoded degrees of freedom is also an important future direction for realizing universal quantum computing.

Furthermore, our formalism opens up new possibilities for experimental implementations of logical quantum computing through real-space geometric manipulations. Note that the lattices in curved manifolds have been implemented in experimental platforms [70–73]. The geometric rotations can be realized via combinations of beam splitters and two-mode squeezing, which are within the current scope of the experimental technology. Our geometric logical gates have good fault tolerance properties since they do not amplify noises. First, they can be realized by two-mode Gaussian operations, which are known to be fault-tolerant for CV codes. Specifically, rotations are isometries of the surfaces, so they preserve the distances and do not amplify position errors. Rotations also commute with the Laplacian. Therefore, they preserve the eigenvalue of the momentum errors, which means a low-energy momentum error remains the same energy. As a result, we expect future exploration of the application of the tessellation codes and geometric gates in quantum experiments to be feasible and valuable.

## ACKNOWLEDGMENT

We thank Victor V. Albert, Anthony Leverrier, Jiuci Xu, Christophe Vuillot, Zhenbin Yang, Ning Bao and Ye Wang for helpful discussions. The unit cell figures on the hyperbolic planes are generated with the assistance of the GAP package HyperCells [74], the Mathematica package HyperBloch [75] and the data of the quotient of triangle groups in Ref. [76]. Y.W. is supported by the National Natural Science Founda-

tion of China Grant No. 12347173, China Postdoctoral Science Foundation Grant No. 2023M742003, and the Shuimu Tsinghua Scholar Program of Tsinghua University. Z.-W.L. is supported in part by a startup funding from YMSC, Tsinghua University, and NSFC under Grant No. 12475023.

## Appendix A: Distances on surfaces and the resolution

In this section, we present the formula for calculating the distances of two points on the sphere and the hyperbolic plane. For the two-dimensional sphere  $S^2$ , we conventionally embed it into the three-dimensional flat space  $\mathbb{R}^3$ :

$$X_1 = \sin \theta \cos \phi, X_2 = \sin \theta \sin \phi, X_3 = \cos \theta, \quad X_1^2 + X_2^2 + X_3^2 = 1, \quad ds^2 = dX_1^2 + dX_2^2 + dX_3^2. \quad (\text{A1})$$

Because the sphere is a homogeneous and isotropic space, to calculate the distance of two arbitrary points on the sphere, we can always find an isometry that transforms one point to  $p_1 = (\theta = 0, \phi = 0)$  and another to a certain  $p_2 = (\theta = \theta_0, \phi = 0)$ . In this case, it is not difficult to calculate the geodesic distance between them as  $\theta_0$ . Note that if we write the res in the embedding coordinate, we have

$$d(p_1, p_2) = \arccos \vec{X}^{(1)} \cdot \vec{X}^{(2)}, \quad (\text{A2})$$

where  $\vec{X}^{(i)} = (\sin \theta \cos \phi, \sin \theta \sin \phi, \cos \theta)|_{p_i}$ . Because the inner product is invariant under any isometry of the sphere, the above expression applies to arbitrary two points on the sphere.

For the hyperbolic surface, it is also convenient to embed it into  $\mathbb{R}^{2,1}$ .

$$X_0 = \cosh \eta, X_1 = \sinh \eta \cos \theta, X_2 = \sinh \eta \sin \theta, \quad -X_0^2 + X_1^2 + X_2^2 = -1, \quad ds^2 = -dX_0^2 + dX_1^2 + dX_2^2. \quad (\text{A3})$$

The resulting line element is  $ds^2 = d\eta^2 + \sinh^2 \eta d\theta^2$ . Because the hyperbolic space is also homogeneous and isotropic, we adopt the same strategy as in the sphere case to calculate the distance between two points. We first transform two points such that  $p_1$  is at the origin,  $p_2$  at  $(\eta_0, \theta = 0)$ . It is easy to calculate their distance in this case as  $\eta_0$ . Writing in terms of the embedding coordinate, it is

$$d(p_1, p_2) = \text{arccosh} (-\vec{X}^{(1)} \cdot \vec{X}^{(2)}), \quad (\text{A4})$$

where  $\vec{X}^{(i)} = (\cosh \eta, \sinh \eta \cos \theta, \sinh \eta \sin \theta)|_{p_i}$  and  $-\vec{X}^{(1)} \cdot \vec{X}^{(2)} = X_0^{(1)} X_0^{(2)} - X_1^{(1)} X_1^{(2)} - X_2^{(1)} X_2^{(2)}$ . Similar to the spherical case, because the inner product is invariant under isometry, this equation applies to any two points in the hyperbolic surface.

One special feature of the hyperbolic plane is that given the values of the three angles  $A, B, C$  of a triangle, its sides are unambiguously determined. This is not the case for the sphere or the Euclidean plane. Let the length of the sides opposite the the corresponding angles be  $a, b, c$ , we have

$$\cosh a = \frac{\cos A + \cos B \cos C}{\sin B \sin C}, \quad \cosh b = \frac{\cos B + \cos C \cos A}{\sin C \sin A}, \quad \cosh c = \frac{\cos C + \cos A \cos B}{\sin A \sin B}. \quad (\text{A5})$$

To calculate the resolution, which is one-half of the minimal distance among any pair of points, we need to get an expression of the distance between points before and after rotating around a point. This can be calculated using Eq. (A2) and (A4). For a point  $p_0$  on the sphere, if rotated around a point  $j$  by angle  $\alpha$  to get  $p_{0j}$ , then  $\vec{X}^{(p_0)} \cdot \vec{X}^{(p_{0j})} = \sin^2 d_{0j} \cos \alpha + \cos^2 d_{0j}$ , where  $d_{0j} = d(p_0, p_j)$ , the distance between  $p_0$  and  $p_j$ . A similar expression in the hyperbolic case is  $\vec{X}^{(p_0)} \cdot \vec{X}^{(p_{0j})} = \cosh^2 d_{0j} - \sinh^2 d_{0j} \cos \alpha$ . To obtain the resolution, it is enough to evaluate the distances of the point  $p_i$  in Eq. (9) with respect to its rotated points after the rotation around  $A, B, C$ . Therefore,

$$d_x = \frac{1}{2} \min\{d(p_i, p_A), d(p_i, p_B), d(p_i, p_C)\}. \quad (\text{A6})$$

Here  $A, B, C$  are the vertices of the triangle and are usually identified with the rotation vertices of the logical operations in specific code constructions.

For a fixed tessellation, one may optimize the choice of the state  $|i\rangle$  in the code construction to maximize the resolution. This is achieved by solving the optimization problem

$$p_i^{(o)} = \underset{p_i}{\text{argmax}} \min\{d(p_i, p_A), d(p_i, p_B), d(p_i, p_C)\}. \quad (\text{A7})$$

For the cases of our interest, the optimal  $p_i^{(o)}$  is a solution of  $d(p_i^{(o)}, p_A) = d(p_i^{(o)}, p_B) = d(p_i^{(o)}, p_C)$ .



## Appendix B: Analysis of the momentum error

We denote the position basis of the two-dimensional surfaces as  $|x\rangle$ , which is normalized to  $\langle x|x'\rangle = \frac{\delta(x_1-x'_1)\delta(x_2-x'_2)}{\sqrt{h(x)}} \equiv \delta^{(2)}(x-x')$ . Here  $h(x)$  is the determinant of the metric evaluated at the point  $x$ . For the sphere, this is  $\langle \theta, \phi|\theta', \phi'\rangle = \frac{\delta(\theta-\theta')\delta(\phi-\phi')}{\sin\theta}$ . For the Euclidean plane, this is the usual  $\langle x, y|x', y'\rangle = \delta(x-x')\delta(y-y')$ . For the hyperbolic plane, this is  $\langle \eta, \theta|\eta', \theta'\rangle = \frac{\delta(\theta-\theta')\delta(\eta-\eta')}{\sinh\eta}$ . If transformed by an isometry  $\rho(g)$  of the surface, the delta function is invariant under the isometry,  $\delta^{(2)}(x-x') = \delta^{(2)}(\rho(g)x - \rho(g)x')$ . Under the position basis, we can write the error operator as

$$\hat{E}_{r,n} = \int d^2x \sqrt{h(x)} \langle x|r, n\rangle |x\rangle \langle x|. \quad (\text{B1})$$

Here  $r$  labels the representation while  $n$  labels the basis in the representation. We match this notation with the momentum errors in Table I. For the sphere,  $r$  is the  $l$  and  $n$  is the  $m$  in  $Y_l^m$ . For the Euclidean plane,  $r$  is  $\{k_x, k_y\}$  and no  $n$  is needed as the representations are one dimensional. For the hyperbolic plane,  $r$  is the  $s$  and  $n$  corresponds to the  $n$  in  $P_{-\frac{1}{2}+is}^n(\cosh\hat{\rho})e^{in\hat{\phi}}$ . We can write the error correction condition as

$$\langle \bar{i}|\hat{E}_{r_1,n_1}^\dagger \hat{E}_{r_2,n_2}|\bar{j}\rangle = \int d^2x \sqrt{h(x)} \langle x|r_2, n_2\rangle \langle r_1, n_1|x\rangle \langle \bar{i}|x\rangle \langle x|\bar{j}\rangle. \quad (\text{B2})$$

Following Eq. (9), we obtain

$$\begin{aligned} \langle x|\bar{j}\rangle &= \sum_{\gamma \in \Gamma} \sum_{g \in G} \langle \Sigma|\rho_L^\dagger(g)|j\rangle \langle x|\rho(\gamma g_0)|p_i\rangle = \sum_{\gamma \in \Gamma} \sum_{g \in G} \langle \Sigma|\rho_L^\dagger(g)|i\rangle \delta^{(2)}(x - \rho(\gamma g_0)p_i), \\ \langle x|\bar{j}\rangle \langle \bar{i}|x\rangle &= \sum_{\gamma_1, \gamma_2 \in \Gamma} \sum_{g_1, g_2 \in G} \langle \Sigma|\rho_L^\dagger(g_1)|j\rangle \langle i|\rho_L(g_2)|\Sigma\rangle \delta^{(2)}(x - \rho(\gamma_1 g_{01})p_i) \delta^{(2)}(x - \rho(\gamma_2 g_{02})p_i) \\ &= \sum_{\gamma \in \Gamma} \sum_{g_1, g_2 \in G} \langle \Sigma|\rho_L^\dagger(g_1)|j\rangle \langle i|\rho_L(g_2)|\Sigma\rangle \delta^{(2)}(x - \rho(\gamma_1 g_{01})p_i) \delta^{(2)}(\rho(\gamma g_{01})p_i - \rho(\gamma g_{02})p_i) \\ &= \sum_{\gamma \in \Gamma} \sum_{g_1, g_2 \in G} \langle \Sigma|\rho_L^\dagger(g_1)|j\rangle \langle i|\rho_L(g_2)|\Sigma\rangle \delta^{(2)}(x - \rho(\gamma g_{01})p_i) \delta^{(2)}(p_i - \rho(g_{01}^{-1}g_{02})p_i) \\ &= \sum_{\gamma \in \Gamma} \sum_{g_1 \in G} \sum_{g_p \in F_{p_i}} \langle \Sigma|\rho_L^\dagger(g_1)|j\rangle \langle i|\rho_L(g_1)\rho_L(g_p)|\Sigma\rangle \delta^{(2)}(x - \rho(\gamma g_{01})p_i) \delta^{(2)}(p_i - p_i) \end{aligned} \quad (\text{B3})$$

Here in the second equality the  $\gamma_1, \gamma_2$  sums reduces to one because different unit cells do not overlap. The third equality follows from the covariance of the  $\delta^{(2)}$  function under an isometry of the surface. The fourth equality follows from a change of summing variable from  $g_2$  to  $g_p$ . The sum over  $g_p$  further reduces from  $G$  to a subgroup which keeps  $p_i$  invariant, denoted as  $F_{p_i}$ . If  $F_{p_i}$  is non trivial, because  $\rho(g_p)p_i = p_i$ , the delta function  $\delta^{(2)}(p_i - \rho(g_p)p_i) = \delta^{(2)}(p_i - p_i)$ . The sum  $\sum_{g_p \in F_{p_i}} \rho_L(g_p)$  is proportional to the projector onto the common eigenvalue 1 subspace of all the group elements  $\rho_L(g_p)$ . As mentioned in Section III A, in this case, we choose  $|\Sigma\rangle$  to be in this subspace and

$$\langle x|\bar{j}\rangle \langle \bar{i}|x\rangle = |F_{p_i}| \delta^{(2)}(p_i - p_i) \sum_{\gamma \in \Gamma} \sum_{g_1 \in G} \langle \Sigma|\rho_L^\dagger(g_1)|j\rangle \langle i|\rho_L(g_1)|\Sigma\rangle \delta^{(2)}(x - \rho(\gamma_1 g_{01})p_i). \quad (\text{B4})$$

If  $F_{p_i}$  is trivial, then  $|F_{p_i}| = 1$  and the above equation also applies, but for an arbitrary  $|\Sigma\rangle$ .

Getting back to Eq. (B2), we obtain

$$\langle \bar{i}|\hat{E}_{r_1,n_1}^\dagger \hat{E}_{r_2,n_2}|\bar{j}\rangle = |F_{p_i}| \delta^{(2)}(p_i - p_i) \sum_{\gamma \in \Gamma} \sum_{g \in G} \langle \Sigma|\rho_L^\dagger(g)|j\rangle \langle i|\rho_L(g)|\Sigma\rangle \langle \rho(\gamma g_0)p_i|r_2, n_2\rangle \langle r_1, n_1|\rho(\gamma g_0)p_i\rangle. \quad (\text{B5})$$

If  $\Gamma$  is trivial, then there is no further simplification to perform and we need to evaluate Eq. (B5) with explicit data of the specific codes. This is the case of Example 1, the calculation of which is in Section B 1. If  $\Gamma$  is nontrivial, then it is a discrete subgroup of the full isometry group of the surface. Recall that  $|r_1, n_1\rangle, |r_2, n_2\rangle$  are the basis of the unitary irreducible representation of the full isometry group. The representations  $r_1, r_2$  are also unitary representations for the subgroup  $\Gamma$ , though they might not be irreducible. Fortunately, in the cases of our interests, when  $\Gamma$  is the translation group on the Euclidean or hyperbolic surface, the representations  $r_1, r_2$  are also irreducible. Therefore, we can first evaluate  $V_\Gamma \equiv \sum_{\gamma \in \Gamma} \rho(\gamma)^{-1} |r_2, n_2\rangle \langle r_1, n_1| \rho(\gamma)$ ,

utilizing the Schur's lemma. There are 3 cases. The first case is  $r_1 = r_2$  and  $n_1 = n_2$ , then  $V_\Gamma = c(r_1, n_1)\mathbb{I}$ . Eq. (B5) is now

$$\begin{aligned}\langle \bar{i} | \hat{E}_{r_1, n_1}^\dagger \hat{E}_{r_1, n_1} | \bar{j} \rangle &= |F_{p_i}| \delta^{(2)}(p_i - p_i) c(r_1, n_1) \sum_{g \in G} \langle \Sigma | \rho_L^\dagger(g) | j \rangle \langle i | \rho_L(g) | \Sigma \rangle \delta^{(2)}(\rho(g_0)p_i - \rho(g_0)p_i) \\ &= |F_{p_i}| |G| \left( \delta^{(2)}(p_i - p_i) \right)^2 c(r_1, n_1) \delta_{i,j}.\end{aligned}\quad (\text{B6})$$

In the second equality, we use the invariance of the  $\delta^{(2)}$  function and the Schur's lemma for the logical group  $G$ . Therefore, the KL condition is satisfied. The second case is that  $r_1, r_2$  are the nonequivalent representations or  $n_1, n_2$  are nonequivalent bases. In this case, the Schur's lemma guarantees that  $\langle \bar{i} | \hat{E}_{r_1, n_1}^\dagger \hat{E}_{r_2, n_2} | \bar{j} \rangle = 0$  for any  $i, j$ . Therefore, the error correction condition is also satisfied. The third case is what may produce the violation of error correction condition. Because  $\Gamma$  is a subgroup of the full isometry group, it is possible that  $|r_1, n_1\rangle, |r_2, n_2\rangle$  different bases for nonequivalent representations for the full isometry group, but become equivalent for the subgroup  $\Gamma$ . In this case, we can formally write Eq. (B5) as

$$\langle \bar{i} | \hat{E}_{r_1, n_1}^\dagger \hat{E}_{r_2, n_2} | \bar{j} \rangle = |F_{p_i}| \left( \delta^{(2)}(p_i - p_i) \right)^2 \sum_{g \in G} c(r_1, n_1, r_2, n_2, g_0 p_i) \langle \Sigma | \rho_L^\dagger(g) | j \rangle \langle i | \rho_L(g) | \Sigma \rangle. \quad (\text{B7})$$

We need to put in data of the specific codes to evaluate whether the error correction condition is violated for particular choices of  $|r_1, n_1\rangle, |r_2, n_2\rangle$ .

In the following, we evaluate the error correction condition explicitly for Examples 1, 2, and 3. Because the error operators are diagonal in the position basis, the two codewords have no spatial overlaps in the above examples, all the terms of the form  $\langle \bar{i} | \hat{E}_{r_1, n_1}^\dagger \hat{E}_{r_2, n_2} | \bar{j} \rangle$  with  $i \neq j$  are zero. We focus on the evaluation of terms  $\langle \bar{i} | \hat{E}_{r_1, n_1}^\dagger \hat{E}_{r_2, n_2} | \bar{i} \rangle$ .

### 1. Momentum error analysis of Example 1

For a generic codewords in Eq. (C1), we can calculate

$$\begin{aligned}\langle \bar{0} | Y_{l_2}^{m_2 \dagger} Y_{l_1}^{m_1} | \bar{0} \rangle &= \frac{1}{4} \left( P_{l_1}^{m_1}(\cos \theta_0) P_{l_2}^{m_2}(\cos \theta_0) e^{i(m_2 - m_1)\phi_0} + P_{l_1}^{m_1}(\cos \theta_0) P_{l_2}^{m_2}(\cos \theta_0) e^{i(m_2 - m_1)(\phi_0 + \pi)} \right. \\ &\quad \left. + P_{l_1}^{m_1}(\cos(\pi - \theta_0)) P_{l_2}^{m_2}(\cos(\pi - \theta_0)) e^{-i(m_2 - m_1)\phi_0} + P_{l_1}^{m_1}(\cos(\pi - \theta_0)) P_{l_2}^{m_2}(\cos(\pi - \theta_0)) e^{i(m_2 - m_1)(\pi - \phi_0)} \right) \\ &= \frac{1}{4} \left( P_{l_1}^{m_1}(\cos \theta_0) P_{l_2}^{m_2}(\cos \theta_0) (1 + (-1)^{m_1 + m_2}) (e^{i(m_2 - m_1)\phi_0} + e^{-i(m_2 - m_1)\phi_0} (-1)^{l_1 + l_2}) \right), \\ \langle \bar{1} | Y_{l_2}^{m_2 \dagger} Y_{l_1}^{m_1} | \bar{1} \rangle &= \frac{1}{4} \left( P_{l_1}^{m_1}(\cos \theta_0) P_{l_2}^{m_2}(\cos \theta_0) (1 + (-1)^{m_1 + m_2}) (e^{i(m_2 - m_1)(\phi_0 + \frac{\pi}{2})} + e^{-i(m_2 - m_1)(\phi_0 + \frac{\pi}{2})} (-1)^{l_1 + l_2}) \right).\end{aligned}\quad (\text{B8})$$

We used the property of the associated Legendre polynomials  $P_l^m(x) = (-1)^{l+m} P_l^m(-x)$  to get the final expression. The expression for  $|\bar{1}\rangle$  is different from that of  $|\bar{0}\rangle$  by  $\phi_0 \rightarrow \phi_0 + \frac{\pi}{2}$ . We immediately see because of the factor  $(1 + (-1)^{m_1 + m_2})$  and the phase difference  $\frac{\pi}{2}$ ,  $\langle \bar{0} | Y_{l_2}^{m_2 \dagger} Y_{l_1}^{m_1} | \bar{0} \rangle \neq \langle \bar{1} | Y_{l_2}^{m_2 \dagger} Y_{l_1}^{m_1} | \bar{1} \rangle$  may only occur when  $(m_2 - m_1) \bmod 4 = 2$ . In this case, we have

$$\langle \bar{0} | Y_{l_2}^{m_2 \dagger} Y_{l_1}^{m_1} | \bar{0} \rangle = -\langle \bar{1} | Y_{l_2}^{m_2 \dagger} Y_{l_1}^{m_1} | \bar{1} \rangle = \frac{1}{2} \left( P_{l_1}^{m_1}(\cos \theta_0) P_{l_2}^{m_2}(\cos \theta_0) (e^{i(m_2 - m_1)\phi_0} + e^{-i(m_2 - m_1)\phi_0} (-1)^{l_1 + l_2}) \right), \quad (\text{B9})$$

In the case we illustrated in Figure 2, we take  $\theta_0 = \arccos \frac{1}{\sqrt{3}}$  and  $\phi_0 = \frac{\pi}{4}$ . In this case, we get  $\langle \bar{0} | Y_{l_2}^{m_2 \dagger} Y_{l_1}^{m_1} | \bar{0} \rangle \propto (1 - (-1)^{l_1 + l_2})$ . Therefore, it is only non-zero when  $l_1 + l_2$  is odd. In summary, the KL condition is only violated when  $l_1 + l_2$  is odd and  $(m_2 - m_1) \bmod 4 = 2$ . Hence,  $Y_1^0 Y_2^{\pm 2}$  is the undetectable error with the smallest  $|l_1| + |l_2| + |m_1| + |m_2| = 5$ .

## 2. Momentum error analysis of Example 2

For the code of Example 2, we calculate the KL condition for a generic code state in Eq. (C2) as

$$\begin{aligned}
& \langle \bar{0} | \hat{V}_{\vec{k}_2}^\dagger \hat{V}_{\vec{k}_1} | \bar{0} \rangle \\
&= \sum_{n_x, n_y \in \mathbb{Z}} e^{4i(n_x \Delta k_x + n_y \Delta k_y)} \left( 4 \cos(\Delta k_x + \Delta k_y) \left( \cos(\Delta k_x - \Delta k_y + x_0 \Delta k_y - y_0 \Delta k_x) + \cos(\Delta k_x + \Delta k_y - x_0 \Delta k_x - y_0 \Delta k_y) \right) \right) \\
&= \delta_{\pi/2}(\Delta k_x) \delta_{\pi/2}(\Delta k_y) \left( 4 \cos(\Delta k_x + \Delta k_y) \left( \cos(\Delta k_x - \Delta k_y + x_0 \Delta k_y - y_0 \Delta k_x) + \cos(\Delta k_x + \Delta k_y - x_0 \Delta k_x - y_0 \Delta k_y) \right) \right), \\
& \cos(\Delta k_x + \Delta k_y) \langle \bar{1} | \hat{V}_{\vec{k}_2}^\dagger \hat{V}_{\vec{k}_1} | \bar{1} \rangle = \cos(\Delta k_x - \Delta k_y) \langle \bar{0} | \hat{V}_{\vec{k}_2}^\dagger \hat{V}_{\vec{k}_1} | \bar{0} \rangle,
\end{aligned} \tag{B10}$$

where  $\Delta k_x = k_{x1} - k_{x2}$ ,  $\Delta k_y = k_{y1} - k_{y2}$ ,  $\delta_{\pi/2}(x) = \sum_{l \in \mathbb{Z}} \delta(x - \frac{l\pi}{2})$ . Because of the delta functions, these two values are non-zero only if  $\Delta k_x, \Delta k_y$  are multiplicities of  $\frac{\pi}{2}$ . Further evaluating the expression when  $\Delta k_x, \Delta k_y$  are multiplicities of  $\frac{\pi}{2}$ , we see that the KL condition is violated only when  $\Delta k_x, \Delta k_y$  are both odd multiplicities of  $\frac{\pi}{2}$ . These circumstances correspond to the logical Pauli  $Z$  operator.

## 3. Momentum error analysis of Example 3

For the codewords of Example 3 in Eq. (C6), the KL condition is written as

$$\begin{aligned}
\langle \bar{0} | \hat{V}_{\vec{k}_2}^\dagger \hat{V}_{\vec{k}_1} | \bar{0} \rangle &= (e^{i\Delta k_x} + e^{-2i\Delta k_x} + e^{i(-\frac{1}{2}\Delta k_x + \frac{3\sqrt{3}}{2}\Delta k_y)}) \sum_{m, n \in \mathbb{Z}} e^{i[(\frac{9}{2}\Delta k_x + \frac{3\sqrt{3}}{2}\Delta k_y)m + 3\sqrt{3}n\Delta k_y]}, \\
&= (e^{i\Delta k_x} + e^{-2i\Delta k_x} + e^{i(-\frac{1}{2}\Delta k_x + \frac{3\sqrt{3}}{2}\Delta k_y)}) \delta_{2\pi}(\frac{9}{2}\Delta k_x + \frac{3\sqrt{3}}{2}\Delta k_y) \delta_{2\pi}(3\sqrt{3}\Delta k_y), \\
\langle \bar{1} | \hat{V}_{\vec{k}_2}^\dagger \hat{V}_{\vec{k}_1} | \bar{1} \rangle &= e^{i(\frac{3}{2}\Delta k_x - \frac{\sqrt{3}}{2}\Delta k_y)} \langle \bar{0} | \hat{V}_{\vec{k}_2}^\dagger \hat{V}_{\vec{k}_1} | \bar{0} \rangle, \\
\langle \bar{2} | \hat{V}_{\vec{k}_2}^\dagger \hat{V}_{\vec{k}_1} | \bar{2} \rangle &= e^{i(-\sqrt{3}\Delta k_y)} \langle \bar{0} | \hat{V}_{\vec{k}_2}^\dagger \hat{V}_{\vec{k}_1} | \bar{0} \rangle.
\end{aligned} \tag{B11}$$

Because of the periodic delta function,  $\langle \bar{0} | \hat{V}_{\vec{k}_2}^\dagger \hat{V}_{\vec{k}_1} | \bar{0} \rangle \neq 0$  only when  $\frac{9}{2}\Delta k_x + \frac{3\sqrt{3}}{2}\Delta k_y = 2m\pi$  and  $3\sqrt{3}\Delta k_y = 2n\pi$ ,  $m, n \in \mathbb{Z}$ . In these cases  $\langle \bar{1} | \hat{V}_{\vec{k}_2}^\dagger \hat{V}_{\vec{k}_1} | \bar{1} \rangle = e^{i\frac{2\pi}{3}(m-n)} \langle \bar{0} | \hat{V}_{\vec{k}_2}^\dagger \hat{V}_{\vec{k}_1} | \bar{0} \rangle$  and  $\langle \bar{2} | \hat{V}_{\vec{k}_2}^\dagger \hat{V}_{\vec{k}_1} | \bar{2} \rangle = e^{-i\frac{2\pi}{3}n} \langle \bar{0} | \hat{V}_{\vec{k}_2}^\dagger \hat{V}_{\vec{k}_1} | \bar{0} \rangle$ . Therefore, the KL condition is violated when either  $m$  or  $n$  is not a multiple of 3. They are equivalent to the cases when both  $3\Delta k_x$  and  $\sqrt{3}\Delta k_y$  are multiplicities of  $\frac{2\pi}{3}$  but not multiplicities of  $2\pi$ , as stated in the main text.

## Appendix C: Further discussion of code examples

In this section, we present and compare other examples of codes based on the same tessellation groups as in Example 1, 2 and 3.

### 1. Codes on $\{2, 2, 4\}$ tessellation

For the code constructed in Example 1, if we choose an arbitrary  $|p_i\rangle = |(\theta_0, \phi_0)\rangle$  in the construction Eq. (9), the most general form of the codewords are

$$\begin{aligned}
|\bar{0}\rangle &= \frac{1}{2}(|\theta_0, \phi_0\rangle + |\pi - \theta_0, -\phi_0\rangle - |\theta_0, \pi + \phi_0\rangle - |\pi - \theta_0, \pi - \phi_0\rangle), \\
|\bar{1}\rangle &= \frac{1}{2}(|\theta_0, \phi_0 + \frac{\pi}{2}\rangle + |\pi - \theta_0, -\phi_0 + \frac{\pi}{2}\rangle - |\theta_0, -\frac{\pi}{2} + \phi_0\rangle - |\pi - \theta_0, -\frac{\pi}{2} - \phi_0\rangle).
\end{aligned} \tag{C1}$$

Here the logical  $Z$  rotates around the  $x$  axis, the logical  $XZ$  rotates around the  $z$  axis and the logical  $X$  rotates around the bisector of the  $x$  and  $y$  axes.

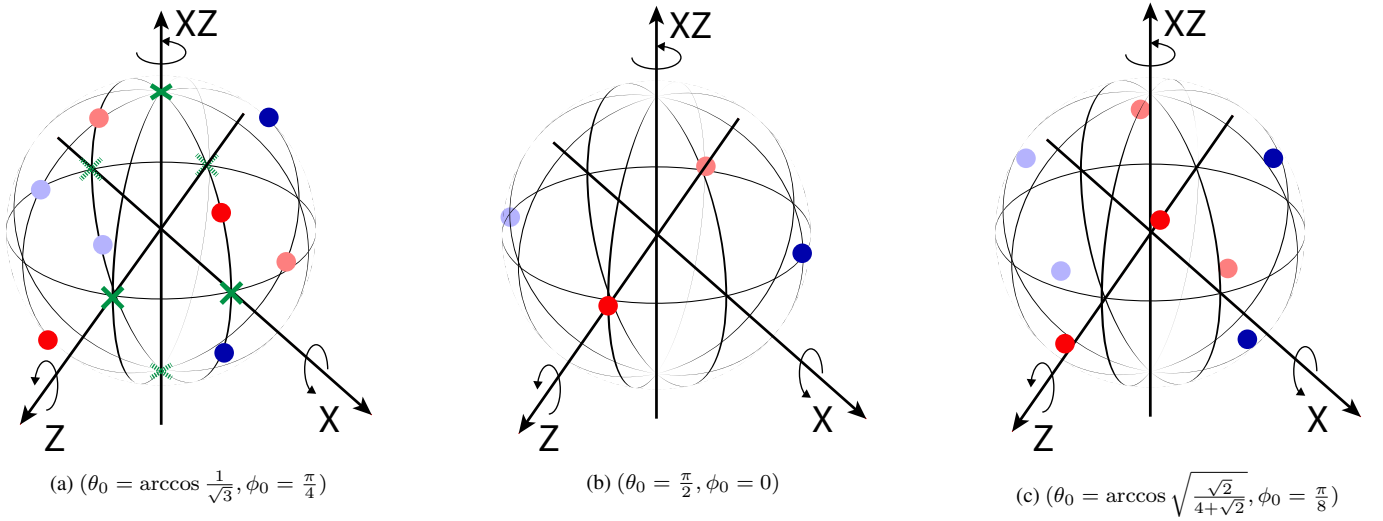


FIG. 5. This figure compares the code constructed from the same encoding map but with a different initial state  $|p_i\rangle$ . The constellation of the spherical code in Example 1, 7 and 8 are shown in subfigures (a), (b) and (c) respectively. The points represent the same as those in Figure 2.

**Example 7.** Here we show another natural choice in which  $\theta_0 = \frac{\pi}{2}$ ,  $\phi_0 = 0$ . The codeword configuration is illustrated in Fig. 5. The logical operations are implemented in the same manner as that in Example 1. The resolution, which is half of the minimal distance between the configuration points is  $\frac{\pi}{4}$ . Therefore, this code can correct any rotation with a rotation angle less than  $\frac{\pi}{4}$ . However, the error correction condition will be violated for those rotations whose axis passes through the states' configuration points, unlike the code in Example 1. For momentum errors, we use Eq. (B8) with  $\theta_0 = \frac{\pi}{2}$ ,  $\phi_0 = 0$ . It is straightforward to find that the lowest error pair that violates the error correction condition is  $Y_0^{0\dagger} Y_2^{\pm 2}$ . So this code can also correct any error with  $l = 1$ .

**Example 8.** If we exclude the cases in which  $|p_i\rangle$  is put on the vertices of rotation, we can solve for the maximal resolution choice of  $|p_i\rangle$  of Eq. A7. The solution is  $\theta_0 = \arccos \sqrt{\frac{\sqrt{2}}{4+\sqrt{2}}}$ ,  $\phi_0 = \frac{\pi}{8}$ . We depict the codeword configuration of this choice of  $|p_i\rangle$  in the right panel of Figure 5. The resolution turns out to be  $d_x = \frac{1}{2} \arccos \frac{\sqrt{2}}{4+\sqrt{2}} \approx 0.6533$ , which is slightly larger than the case in Example 1, where  $d_x = \frac{1}{2} \arccos \frac{1}{3} \approx 0.6155$ . This code corrects any rotation error whose rotation angle is less than the resolution  $d_x \approx 0.6533$ . But similar to Example 7, it does not correct the errors when the rotation axis of  $R_2^\dagger R_1$  passes through any codeword configuration point. For the momentum error, plugging  $\theta_0 = \arccos \sqrt{\frac{\sqrt{2}}{4+\sqrt{2}}}$ ,  $\phi_0 = \frac{\pi}{8}$  into Eq. (B9), we see that the error correction condition is violated when  $(m_2 - m_1) \bmod 4 = 2$ .

## 2. Codes on $\{2, 4, 4\}$ tessellation

For the code construction in Figure 2, if we take the  $(XZ)^{-1}$  rotation vertex as  $(0, 0)$ , for a generic  $|p_1\rangle = |(x_0, y_0)\rangle$ , the unnormalized codewords are

$$\begin{aligned}
 |\bar{0}\rangle &= \sum_{m,n \in \mathbb{Z}} |(4m + x_0, 4n + y_0)\rangle + |(4m + 2 - y_0, 4n + x_0)\rangle + |(4m + y_0, 4n + 2 - x_0)\rangle + |(4m + 2 - x_0, 4n + 2 - y_0)\rangle \\
 &\quad - |(4m - x_0, 4n - y_0)\rangle - |(4m - 2 + y_0, 4n - x_0)\rangle - |(4m - y_0, 4n - 2 + x_0)\rangle - |(4m - 2 + x_0, 4n - 2 + y_0)\rangle, \\
 |\bar{1}\rangle &= \sum_{m,n \in \mathbb{Z}} |(4m + x_0, 4n + y_0 - 2)\rangle + |(4m + 2 - y_0, 4n + x_0 - 2)\rangle + |(4m + y_0, 4n - x_0)\rangle + |(4m + 2 - x_0, 4n - y_0)\rangle \\
 &\quad - |(4m - x_0, 4n - y_0 + 2)\rangle - |(4m - 2 + y_0, 4n - x_0 + 2)\rangle - |(4m - y_0, 4n + x_0)\rangle - |(4m - 2 + x_0, 4n + y_0)\rangle.
 \end{aligned} \tag{C2}$$

As mentioned in the main text, each mode in the  $x$  or  $y$  direction is a one-dimensional GKP code. Its code words are

$$|k\rangle_{\text{GKP}} = \sum_{n \in \mathbb{Z}} |4n + 2k + \frac{1}{2}\rangle + |4n + 2k + \frac{3}{2}\rangle, \quad k \in \{0, 1\}. \quad (\text{C3})$$

The GKP stabilizers for each mode are  $\hat{S}_q = e^{i2\pi(\hat{q} - \frac{1}{2})}$  and  $\hat{S}_p = e^{i4\hat{p}}$ . The GKP logical operators are  $X_{\text{GKP}} = e^{i2\hat{p}}$ ,  $Z_{\text{GKP}} = \sqrt{2} \sin \frac{\pi}{2} \hat{q}$ . The codewords in Eq. (C2) can be written as

$$|\bar{0}\rangle = \frac{1}{\sqrt{2}}(|0\rangle_{\text{GKP}}^{(x)}|0\rangle_{\text{GKP}}^{(y)} - |1\rangle_{\text{GKP}}^{(x)}|1\rangle_{\text{GKP}}^{(y)}), \quad |\bar{1}\rangle = \frac{1}{\sqrt{2}}(|0\rangle_{\text{GKP}}^{(x)}|1\rangle_{\text{GKP}}^{(y)} - |1\rangle_{\text{GKP}}^{(x)}|0\rangle_{\text{GKP}}^{(y)}). \quad (\text{C4})$$

This is a 2-to-1 concatenated GKP code with stabilizers and logical operators

$$S = -X_{\text{GKP}}^{(x)}X_{\text{GKP}}^{(y)}, \quad L_X = -X_{\text{GKP}}^{(x)} = X_{\text{GKP}}^{(y)}, \quad L_Z = Z_{\text{GKP}}^{(x)}Z_{\text{GKP}}^{(y)}. \quad (\text{C5})$$

### 3. Codes on $\{3, 3, 3\}$ tessellation

Taking the origin at the vertex of  $(ZX)^{-1}$ , the two vectors generating the translation symmetry of the lattice are  $\vec{v}_1 = (0, 3\sqrt{3})$  and  $\vec{v}_2 = (\frac{9}{2}, \frac{3\sqrt{3}}{2})$ . The codewords can be written as

$$\begin{aligned} |\bar{0}\rangle &= \sum_{m,n \in \mathbb{Z}} \left( |(1, 0)\rangle + \omega |(-\frac{1}{2}, \frac{3\sqrt{3}}{2})\rangle + \omega^2 |(-2, 0)\rangle \right) (m\vec{v}_1 + n\vec{v}_2), \\ |\bar{1}\rangle &= \sum_{m,n \in \mathbb{Z}} \left( |(1, \sqrt{3})\rangle + \omega |(-\frac{1}{2}, -\frac{\sqrt{3}}{2})\rangle + \omega^2 |(\frac{5}{2}, -\frac{\sqrt{3}}{2})\rangle \right) (m\vec{v}_1 + n\vec{v}_2), \\ |\bar{2}\rangle &= \sum_{m,n \in \mathbb{Z}} \left( |(-\frac{1}{2}, \frac{\sqrt{3}}{2})\rangle + \omega |(-2, -\sqrt{3})\rangle + \omega^2 |(1, -\sqrt{3})\rangle \right) (m\vec{v}_1 + n\vec{v}_2), \end{aligned} \quad (\text{C6})$$

where  $\omega = e^{i\frac{2\pi}{3}}$ . By  $(m\vec{v}_1 + n\vec{v}_2)$  we mean translating the points in the previous parenthesis by  $m\vec{v}_1 + n\vec{v}_2$ . This code has GKP-like stabilizer operators. The stabilizers are

$$\hat{S}_{p,1} = e^{i3\sqrt{3}\hat{p}_y}, \quad \hat{S}_{p,2} = e^{i(\frac{9}{2}\hat{p}_x + \frac{3\sqrt{3}}{2}\hat{p}_y)}, \quad \hat{S}_{q,1} = e^{i\frac{4\pi}{\sqrt{3}}\hat{q}}, \quad \hat{S}_{q,2} = e^{i(\frac{2\pi}{3}(\hat{x}-1) + \frac{2\pi}{\sqrt{3}}\hat{y})}. \quad (\text{C7})$$

The GKP-like logical  $Z$  operator is  $L_Z = e^{i\frac{4\pi}{3\sqrt{3}}\hat{y}}$  and its stabilizer equivalence. However, the logical  $X$  operator cannot be realized by real space displacement.

### Appendix D: Figures of code state constellations

In this section, we collect the figures (Figures 6, 7 and 8) which illustrate the code state constellation configurations in Examples 4, 5 and 6, respectively.

- 
- |   |  |
|---|--|
| <p>[1] H. Bombín, Gauge color codes: optimal transversal gates and gauge fixing in topological stabilizer codes, <i>New Journal of Physics</i> <b>17</b>, 083002 (2015).</p> <p>[2] M. S. Kesselring, F. Pastawski, J. Eisert, and B. J. Brown, The boundaries and twist defects of the color code and their applications to topological quantum computation, <i>Quantum</i> <b>2</b>, 101 (2018).</p> <p>[3] M. Vasmer and D. E. Browne, Three-dimensional surface</p> | <p>codes: Transversal gates and fault-tolerant architectures, <i>Phys. Rev. A</i> <b>100</b>, 012312 (2019).</p> <p>[4] T. Jochym-O'Connor and T. J. Yoder, Four-dimensional toric code with non-clifford transversal gates, <i>Phys. Rev. Res.</i> <b>3</b>, 013118 (2021).</p> <p>[5] G. Zhu, T. Jochym-O'Connor, and A. Dua, Topological order, quantum codes, and quantum computation on fractal geometries, <i>PRX Quantum</i> <b>3</b>, 030338 (2022).</p> |
|---|--|



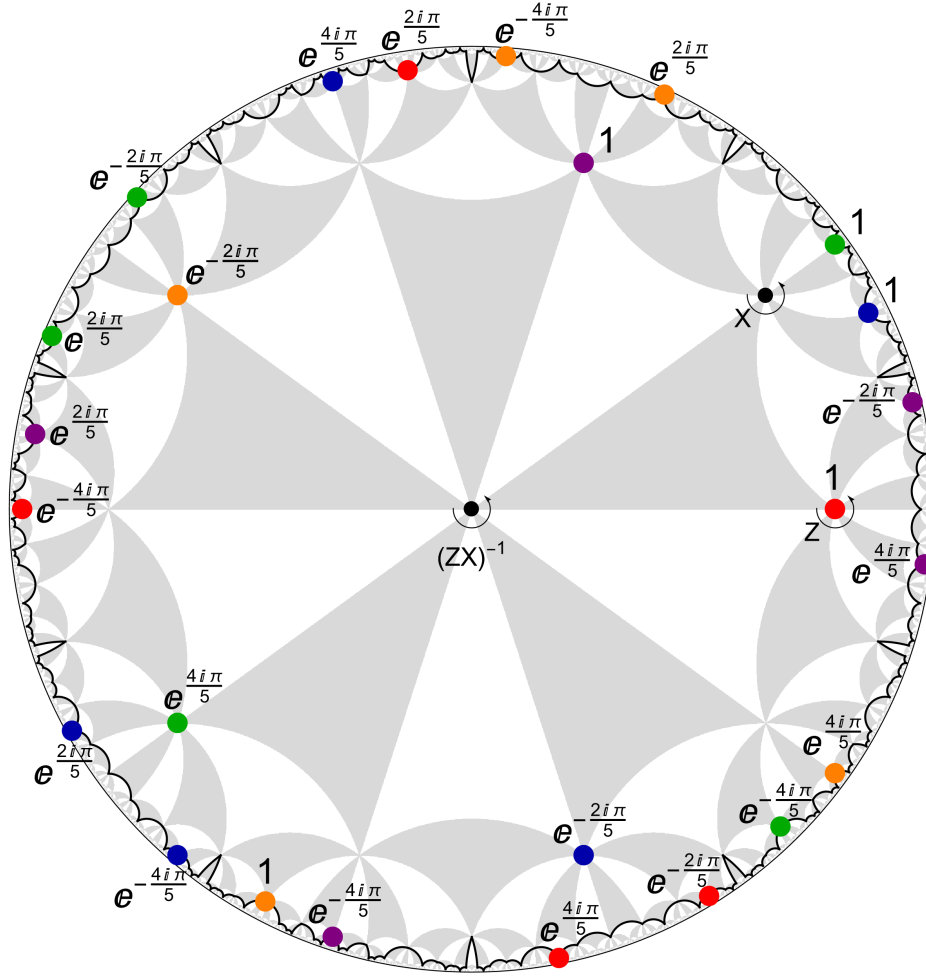


FIG. 6. The constellation of the hyperbolic code in Example 4, designed to realize  $\mathbb{Z}_5$  qudit Pauli group via rotation. The red, blue, green, orange and purple colours label the logical  $|\bar{0}\rangle$  to  $|\bar{4}\rangle$  respectively. The coefficients in the superposition are labelled next to the point.

- [6] G. Zhu, S. Sikander, E. Portnoy, A. W. Cross, and B. J. Brown, Non-clifford and parallelizable fault-tolerant logical gates on constant and almost-constant rate homological quantum ldpc codes via higher symmetries, [arXiv preprint arXiv:2310.16982 \(2023\)](#).
- [7] M. S. Kesselring, J. C. Magdalena de la Fuente, F. Thomsen, J. Eisert, S. D. Bartlett, and B. J. Brown, Anyon condensation and the color code, [PRX Quantum 5, 010342 \(2024\)](#).
- [8] A. Krishna and D. Poulin, Fault-tolerant gates on hypergraph product codes, [Phys. Rev. X 11, 011023 \(2021\)](#).
- [9] Q. Xu, H. Zhou, G. Zheng, D. Bluvstein, J. Ataiades, M. D. Lukin, and L. Jiang, Fast and parallelizable logical computation with homological product codes, [arXiv preprint arXiv:2407.18490 \(2024\)](#).
- [10] P. Faist, S. Nezami, V. V. Albert, G. Salton, F. Pastawski, P. Hayden, and J. Preskill, Continuous symmetries and approximate quantum error correction, [Phys. Rev. X 10, 041018 \(2020\)](#).
- [11] M. P. Woods and A. M. Alhambra, Continuous groups of transversal gates for quantum error correcting codes from finite clock reference frames, [Quantum 4, 245 \(2020\)](#).
- [12] S. Zhou, Z.-W. Liu, and L. Jiang, New perspectives on covariant quantum error correction, [Quantum 5, 521 \(2021\)](#).
- [13] A. Kubica and R. Demkowicz-Dobrzański, Using quantum metrological bounds in quantum error correction: A simple proof of the approximate eastin-knill theorem, [Phys. Rev. Lett. 126, 150503 \(2021\)](#).
- [14] Z.-W. Liu and S. Zhou, Quantum error correction meets continuous symmetries: fundamental trade-offs and case studies, [arXiv preprint arXiv:2111.06360 \(2021\)](#).
- [15] L. Kong and Z.-W. Liu, Near-optimal covariant quantum error-correcting codes from random unitaries with symmetries, [PRX Quantum 3, 020314 \(2022\)](#).
- [16] Y. Yang, Y. Mo, J. M. Renes, G. Chiribella, and M. P. Woods, Optimal universal quantum error correction via bounded reference frames, [Phys. Rev. Res. 4, 023107 \(2022\)](#).
- [17] Z.-W. Liu and S. Zhou, Approximate symmetries and quantum error correction, [npj Quantum Information 9, 119 \(2023\)](#).
- [18] D. Gottesman, A. Kitaev, and J. Preskill, Encoding a qubit in an oscillator, [Phys. Rev. A 64, 012310 \(2001\)](#).
- [19] K. Noh and C. Chamberland, Fault-tolerant bosonic quantum error correction with the surface–gottesman-kitaev-preskill code, [Phys. Rev. A 101, 012316 \(2020\)](#).
- [20] B. Q. Baragiola, G. Pantaleoni, R. N. Alexander, A. Karanjai,

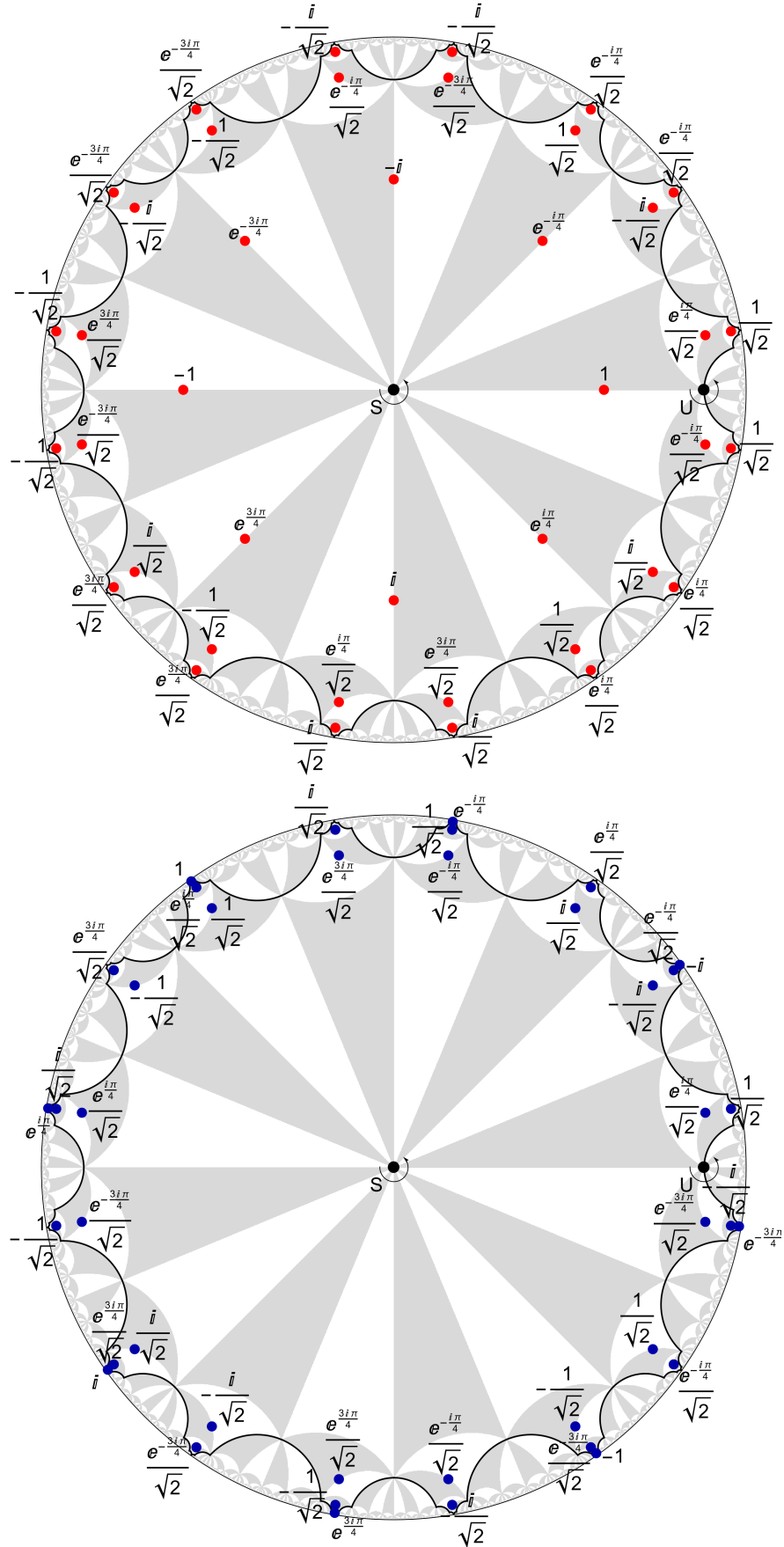


FIG. 7. The upper and lower graphs illustrate the codeword configuration of the logical  $|\bar{0}\rangle$  and  $|\bar{1}\rangle$  states for the construction in Example 5 respectively. Each codeword has a superposition of 40 points in one unit cell. The coefficients of the superposition are labelled next to the points.

- and N. C. Menicucci, All-gaussian universality and fault tolerance with the Gottesman-Kitaev-Preskill code, *Phys. Rev. Lett.* **123**, 200502 (2019).
- [21] C. Calcluth, N. Reichel, A. Ferraro, and G. Ferrini, Sufficient condition for universal quantum computation using bosonic circuits, *PRX Quantum* **5**, 020337 (2024).
- [22] S. Krastanov, V. V. Albert, C. Shen, C.-L. Zou, R. W. Heeres, B. Vlastakis, R. J. Schoelkopf, and L. Jiang, Universal control of an oscillator with dispersive coupling to a qubit, *Phys. Rev. A* **92**, 040303 (2015).
- [23] R. W. Heeres, P. Reinhold, N. Ofek, L. Frunzio, L. Jiang, M. H. Devoret, and R. J. Schoelkopf, Implementing a universal gate set on a logical qubit encoded in an oscillator, *Nature communications* **8**, 94 (2017).
- [24] J. Guillaud and M. Mirrahimi, Repetition cat qubits for fault-tolerant quantum computation, *Phys. Rev. X* **9**, 041053 (2019).
- [25] T. Hillmann, F. Quijandría, G. Johansson, A. Ferraro, S. Gasparinetti, and G. Ferrini, Universal gate set for continuous-variable quantum computation with microwave circuits, *Phys. Rev. Lett.* **125**, 160501 (2020).
- [26] M. Davydova, N. Tantivasadakarn, S. Balasubramanian, and D. Aasen, Quantum computation from dynamic automorphism codes, *Quantum* **8**, 1448 (2024).
- [27] R. Kobayashi and G. Zhu, Cross-cap defects and fault-tolerant logical gates in the surface code and the honeycomb Floquet code, *PRX Quantum* **5**, 020360 (2024).
- [28] X. Fu and D. Gottesman, Error correction in dynamical codes (2024), [arXiv:2403.04163 \[quant-ph\]](https://arxiv.org/abs/2403.04163).
- [29] S. Bartolucci, P. Birchall, H. Bombin, H. Cable, C. Dawson, M. Gimeno-Segovia, E. Johnston, K. Kieling, N. Nickerson, M. Pant, *et al.*, Fusion-based quantum computation, *Nature Communications* **14**, 912 (2023).
- [30] H. Bombin, C. Dawson, R. V. Mishmash, N. Nickerson, F. Pastawski, and S. Roberts, Logical blocks for fault-tolerant topological quantum computation, *PRX Quantum* **4**, 020303 (2023).
- [31] V. V. Albert, J. P. Covey, and J. Preskill, Robust encoding of a qubit in a molecule, *Phys. Rev. X* **10**, 031050 (2020).
- [32] J. A. Gross, Designing codes around interactions: The case of a spin, *Phys. Rev. Lett.* **127**, 010504 (2021).
- [33] S. Omanakuttan and J. A. Gross, Multispin Clifford codes for angular momentum errors in spin systems, *Phys. Rev. A* **108**, 022424 (2023).
- [34] S. P. Jain, J. T. Iosue, A. Barg, and V. V. Albert, Quantum spherical codes, *Nature Physics* **1**, 1 (2024).
- [35] A. Denys and A. Leverrier, The  $2t$ -qutrit, a two-mode bosonic qutrit, *Quantum* **7**, 1032 (2023).
- [36] A. Denys and A. Leverrier, Quantum error-correcting codes with a covariant encoding, *Phys. Rev. Lett.* **133**, 240603 (2024).
- [37] E. Kubischta and I. Teixeira, Family of quantum codes with exotic transversal gates, *Phys. Rev. Lett.* **131**, 240601 (2023).
- [38] E. Kubischta and I. Teixeira, Permutation-invariant quantum codes with transversal generalized phase gates, [arXiv preprint arXiv:2310.17652](https://arxiv.org/abs/2310.17652) (2023).
- [39] E. Kubischta and I. Teixeira, Quantum codes and irreducible products of characters, [arXiv preprint arXiv:2403.08999](https://arxiv.org/abs/2403.08999) (2024).
- [40] N. P. Breuckmann and S. Burton, Fold-transversal Clifford gates for quantum codes, *Quantum* **8**, 1372 (2024).
- [41] J. Conrad, J. Eisert, and F. Arzani, Gottesman-Kitaev-Preskill codes: A lattice perspective, *Quantum* **6**, 648 (2022).
- [42] J. Conrad, A. G. Burchards, and S. T. Flammia, Lattices, gates, and curves: GKP codes as a Rosetta stone, [arXiv preprint arXiv:2407.03270](https://arxiv.org/abs/2407.03270) (2024).
- [43] F. Pastawski, B. Yoshida, D. Harlow, and J. Preskill, Holographic quantum error-correcting codes: Toy models for the bulk/boundary correspondence, *Journal of High Energy Physics* **2015**, 1 (2015).
- [44] L. Boyle, M. Dickens, and F. Flicker, Conformal quasicrystals and holography, *Phys. Rev. X* **10**, 011009 (2020).
- [45] L. Boyle and J. Kulp, Holographic foliations: Self-similar quasicrystals from hyperbolic honeycombs, [arXiv preprint arXiv:2408.15316](https://arxiv.org/abs/2408.15316) (2024).
- [46] Z. Li and L. Boyle, The Penrose tiling is a quantum error-correcting code, [arXiv preprint arXiv:2311.13040](https://arxiv.org/abs/2311.13040) (2023).
- [47] E. B. da Silva, M. Firer, S. R. Costa, and R. Palazzo Jr, Signal constellations in the hyperbolic plane: A proposal for new communication systems, *Journal of the Franklin Institute* **343**, 69 (2006).
- [48] S. Bravyi, D. Poulin, and B. Terhal, Tradeoffs for reliable quantum information storage in 2d systems, *Phys. Rev. Lett.* **104**, 050503 (2010).
- [49] N. P. Breuckmann and B. M. Terhal, Constructions and noise threshold of hyperbolic surface codes, *IEEE Transactions on Information Theory* **62**, 3731 (2016).
- [50] N. P. Breuckmann, C. Vuillot, E. Campbell, A. Krishna, and B. M. Terhal, Hyperbolic and semi-hyperbolic surface codes for quantum storage, *Quantum Science and Technology* **2**, 035007 (2017).
- [51] J. Maciejko and S. Rayan, Hyperbolic band theory, *Science advances* **7**, eabe9170 (2021).
- [52] J. Maciejko and S. Rayan, Automorphic Bloch theorems for hyperbolic lattices, *Proceedings of the National Academy of Sciences* **119**, e2116869119 (2022).
- [53] P. M. Lenggenhager, J. Maciejko, and T. c. v. Bzdušek, Non-abelian hyperbolic band theory from supercells, *Phys. Rev. Lett.* **131**, 226401 (2023).
- [54] I. Boettcher, A. V. Gorshkov, A. J. Kollár, J. Maciejko, S. Rayan, and R. Thomale, Crystallography of hyperbolic lattices, *Physical Review B* **105**, 125118 (2022).
- [55] P. Bienias, I. Boettcher, R. Belyansky, A. J. Kollár, and A. V. Gorshkov, Circuit quantum electrodynamics in hyperbolic space: From photon bound states to frustrated spin models, *Phys. Rev. Lett.* **128**, 013601 (2022).
- [56] A. Stegmaier, L. K. Upreti, R. Thomale, and I. Boettcher, Universality of Hofstadter butterflies on hyperbolic lattices, *Phys. Rev. Lett.* **128**, 166402 (2022).
- [57] D. M. Urwyler, P. M. Lenggenhager, I. Boettcher, R. Thomale, T. Neupert, and T. c. v. Bzdušek, Hyperbolic topological band insulators, *Phys. Rev. Lett.* **129**, 246402 (2022).
- [58] A. Chen, J. Maciejko, and I. Boettcher, Anderson localization transition in disordered hyperbolic lattices, *Phys. Rev. Lett.* **133**, 066101 (2024).
- [59] T. Tummuru, A. Chen, P. M. Lenggenhager, T. Neupert, J. Maciejko, and T. Bzdušek, Hyperbolic non-abelian semimetal, *Physical Review Letters* **132**, 206601 (2024).
- [60] H. S. Coxeter and W. O. Moser, *Generators and relations for discrete groups*, Vol. 14 (Springer Science & Business Media, 2013).
- [61] W. Magnus, *Noneuclidean tessellations and their groups*, Vol. 61 (Academic Press, 1974).
- [62] E. Knill and R. Laflamme, Theory of quantum error-correcting codes, *Phys. Rev. A* **55**, 900 (1997).
- [63] P. C. Yang and S.-T. Yau, Eigenvalues of the Laplacian of compact Riemann surfaces and minimal submanifolds, *Annali della Scuola Normale Superiore di Pisa - Classe di Scienze Ser. 4*, **7**, 55 (1980).
- [64] O. Parzanchevski and P. Sarnak, Super-golden-gates for  $pu(2)$ ,

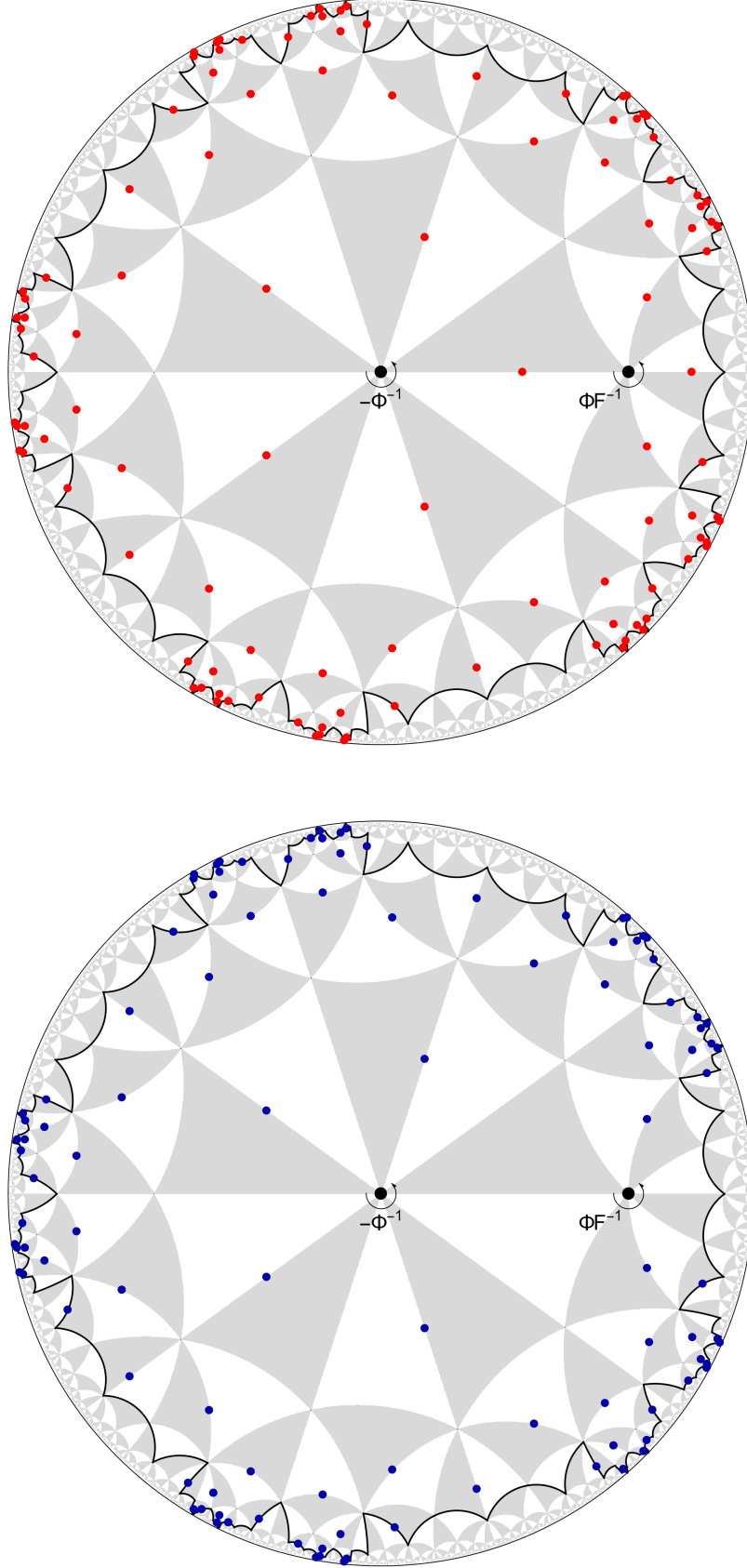


FIG. 8. The upper and lower graphs illustrate the codeword configuration of the logical  $|\bar{0}\rangle$  and  $|\bar{1}\rangle$  states Example 6 respectively.

- Advances in Mathematics* **327**, 869 (2018), special volume honoring David Kazhdan.
- [65] P. Hayden, S. Nezami, S. Popescu, and G. Salton, Error correction of quantum reference frame information, *PRX Quantum* **2**, 010326 (2021).
  - [66] B. Eastin and E. Knill, Restrictions on transversal encoded quantum gate sets, *Phys. Rev. Lett.* **102**, 110502 (2009).
  - [67] O. Hahn, A. Ferraro, L. Hultquist, G. Ferrini, and L. García-Álvarez, Quantifying qubit magic resource with gottesman-kitaev-preskill encoding, *Phys. Rev. Lett.* **128**, 210502 (2022).
  - [68] L. Feng and S. Luo, Connecting continuous and discrete wigner functions via gkp encoding, *International Journal of Theoretical Physics* **63**, 40 (2024).
  - [69] O. Hahn, G. Ferrini, and R. Takagi, Bridging magic and non-gaussian resources via gottesman-kitaev-preskill encoding, *arXiv preprint arXiv:2406.06418* (2024).
  - [70] D. Barredo, V. Lienhard, S. De Leseleuc, T. Lahaye, and A. Browaeys, Synthetic three-dimensional atomic structures assembled atom by atom, *Nature* **561**, 79 (2018).
  - [71] A. J. Kollár, M. Fitzpatrick, and A. A. Houck, Hyperbolic lattices in circuit quantum electrodynamics, *Nature* **571**, 45 (2019).
  - [72] P. M. Lenggenhager, A. Stegmaier, L. K. Upreti, T. Hofmann, T. Helbig, A. Vollhardt, M. Greiter, C. H. Lee, S. Imhof, H. Brand, *et al.*, Simulating hyperbolic space on a circuit board, *Nature communications* **13**, 4373 (2022).
  - [73] A. Chen, H. Brand, T. Helbig, T. Hofmann, S. Imhof, A. Fritzsche, T. Kießling, A. Stegmaier, L. K. Upreti, T. Neupert, *et al.*, Hyperbolic matter in electrical circuits with tunable complex phases, *Nature Communications* **14**, 622 (2023).
  - [74] P. M. Lenggenhager, J. Maciejko, and T. Bzdušek, *HyperCells: A GAP package for constructing primitive cells and supercells of hyperbolic lattices* (2023), <https://github.com/patrick-lenggenhager/HyperCells>.
  - [75] P. M. Lenggenhager, J. Maciejko, and T. Bzdušek, *HyperBloch: A Mathematica package for hyperbolic tight-binding models and the supercell method* (2023), <https://github.com/patrick-lenggenhager/HyperBloch>.
  - [76] M. Conder, Quotients of triangle groups acting on surfaces of genus 2 to 101, <https://www.math.auckland.ac.nz/~conder/TriangleGroupQuotients101.txt> (2007).